Journal of Building Engineering 104 (2025) 112229

Contents lists available at ScienceDirect

Journal of Building Engineering

journal homepage: www.elsevier.com/locate/jobe

Stress and damage distribution analysis of steel reinforced geopolymer concrete beams: Finite element method and experimental comparison under varying design parameters

Ahmet Özbayrak [a,*], Hurmet Kucukgoncu [b], Huseyin Hilmi Aslanbay [a], Yuksel Gul Aslanbay [a]

[a] Erciyes University, Engineering Faculty, Civil Engineering Department, Kayseri, Türkiye
[b] Abdullah Gül University, Engineering Faculty, Civil Engineering Department, Kayseri, Türkiye

ARTICLE INFO

Keywords:
Geopolymer reinforced concrete beam
Experimental and numerical study
Structural behavior
FEA
Stress and damage distribution

ABSTRACT

Geopolymer concrete (GPC) is a sustainable and eco-friendly alternative to ordinary Portland cement-based concrete (OPC). However, its application in reinforced concrete structures remains limited due to insufficient research on structural performance. This study examines the effects of tensile reinforcement ratio, sodium silicate/sodium hydroxide ratio, and curing method on GPC-reinforced concrete (GPC-RC) beams. Experimental and numerical bending tests were performed on GPC and OPC beams with similar tensile reinforcement and strength properties. Load-displacement and moment-curvature relationships were obtained and compared, while stress and stiffness behaviors were analyzed numerically. The results show that curing methods and reinforcement ratios significantly influence GPC beam behavior. In GPC samples, numerical and experimental displacement and load values differed by approximately 10 % at both yield and ultimate points. For OPC, these differences were 35 % and 14 % at the yield point and 17 % and 25 % at the ultimate point. GPC exhibited distinct stress and damage distribution characteristics compared to OPC. The finite element models were statistically validated, confirming their consistency with experimental results. These findings contribute to the understanding of GPC's structural behavior and provide guidance for its design and optimization in reinforced concrete applications.

Nomenclature and abbreviations

GPC	Geopolymer concrete	f_{b0}/f_{c0}	The ratio of initial equibiaxial compressive yield stress to initial uniaxial compressive yield stress.
OPC	Ordinary Portland Concrete	**K**	K_c, the ratio of the second stress invariant on the tensile meridian
FEM	Finite Element Method	φ	Dilation angle
SS	Sodium Silicate	υ	Viscosity parameter
SH	Sodium Hydroxide	ϵ	Eccentricity
RC	Reinforced Concrete	ε_c	Strain of concrete
FEA	Finite Element Analysis	ε_c^{in}	Inelastic strain of concrete
CFRP	Carbon-Fiber- Reinforced Polymer	σ_c	Compression stress of concrete

(*continued on next page*)

* Corresponding author.
E-mail address: ozbayrak@erciyes.edu.tr (A. Özbayrak).

https://doi.org/10.1016/j.jobe.2025.112229
Received 12 November 2024; Received in revised form 6 February 2025; Accepted 27 February 2025
Available online 7 March 2025

(*continued*)

SDEG	Scaler Stifness Degradation	E_0	Elastic modulus of concrete
AA	Sum of SS and SH	d_c	Damage parameter of concrete
FA	Fly Ash	ε_c^{pl}	Plastic strain of concrete
GB	Geopolymer Beam	b_c	The ratio of plastic strain to inelastic strain
OPCB	Ordinary Portland Concrete Beam	σ_t	Tension stress
C0	Direct Heat-Curing	f_{ct}	Concrete tension strength
C4	Heat-Curing After 4 Days	w_o	Crack width
F	SS/SH	Δ	Displacement
C3D8R	Eight-node hexahedral elements	d_c	Damage parameter
T3D2	A model 3D bar finite elements with two nodes and one degree of freedom	b_t	The ratio of plastic strain to inelastic strain

1. Introduction

Nowadays, studies on geopolymer concrete (GPC) have become quite widespread, and researchers make great efforts to use a more environmentally friendly and sustainable building material instead of ordinary Portland cement concrete (OPC). GPC offers big advantages in terms of reducing carbon footprint and utilizing waste materials; therefore, it becomes an increasingly attractive alternative for the construction sector. These studies aim to contribute to more sustainable construction practices by providing both environmental and economic benefits [1]. According to many experimental studies, the low elastic modulus of geopolymer concrete changes its deformation properties in terms of behavior, but it can carry equivalent loads to traditional concrete in terms of strength. This shows that GPC increases its flexibility and allows larger deformation while maintaining its structural durability and load-bearing capacity. These features create significant differences in structural performance, especially under earthquakes and other dynamic loads [2]. In addition to its mechanical properties, the dense micro-level porosity determined in microstructural studies also highlights GPC in terms of dynamic properties by increasing damping. This dense porosity increases the energy absorption capacity of the material under dynamic loads such as vibration and impact, thus improving the durability and performance of structures. These properties make GPC a suitable alternative, especially for earthquake zones and structures exposed to high dynamic loads [3]. In addition, the ratios of sodium hydroxide (SH) and sodium silicate (SS) solutions, which provide alkali activation in GPC, to each other and to fly ash lead to some differences in the behavior and strength of geopolymer concrete. Changes in the ratios of these solutions affect the mechanical and dynamic properties of the concrete, causing it to perform differently under different loads. Determining the correct ratios is critical to optimizing properties of the concrete, such as compressive and tensile strength, elastic modulus, and damping capacity. Correct adjustment of these factors can improve the performance and expand application areas of GPC [4]. GPC provides much better adhesion to the reinforcement than traditional concrete due to the strong bonding forces of alkali activators. These strong bonding forces increase the interaction between the reinforcement and the concrete, improving structural integrity and durability. As a result, GPC provides better adhesion with the reinforcement and shows higher performance, especially against tensile and shear forces. This feature makes it preferred in the construction of more reliable and durable structures under earthquakes and other dynamic loads [5]. In addition, GPC can maintain its strength even when exposed to high temperatures thanks to its low water content. Low water content reduces the amount of water in the concrete, while at the same time causing less water evaporation and water vapor pressure. This increases the durability and thermal stability of the concrete under high temperature. As a result, GPC maintains its durability even at high temperatures, making it a more reliable structural material under fire and other thermal loads [6]. All of these mentioned studies are carried out with great effort in terms of time and cost. However, in the light of the experience and knowledge gained, studies can be progressed more quickly and reliably by calibrating and simulating existing information. This can enable geopolymer concrete to enter our daily lives more quickly. The results obtained from methods such as finite element analysis (FEA) can enable more detailed investigation of behaviors that cannot be followed in experiments and contribute to the form of specifications in this direction. These approaches can accelerate studies on the development of more effective and sustainable building materials in the future.

In the studies, it was stated that the FEA geometry created using the real material model can realistically analyze the behavior of geopolymer reinforced concrete (GPC-RC) beams and show the behavior of the structural element up to collapse [7–9]. Studies revealed that the FEA model accurately predicts high load-bearing capacity, but the behavior under increasing load may deviate from the experimental data [10]. The differences between the experimental and FEA results become more apparent, especially at higher load rates. Small differences in peak strength values were observed between the experimental findings and the finite element model results. In particular, a 4 % difference in peak values and a 10 % difference in strength values were found for GPC. These differences may be due to the friction forces occurring during the tests [11]. In the study by Chong et al. the FEA results generally provided higher load capacity than the experimental results. However, it was observed that the FEA results showed more asymmetry than expected in the load-displacement curve, which can be considered under increasing bending moment. However, the results of both methods were found to be similar in terms of stiffness degradation, energy consumption and ductility. Experimental results for moment-curvature plots showed a smoother behavior, while FEA results showed a sharp behavior [12]. Selecting the right mesh size is a factor that can help in better estimating the ultimate load-bearing capacity of structures. A smaller mesh size brings the FEA results closer to the experimental results, while a larger mesh size produces larger differences between the results [13]. The FEA results obtained by Nofal et al. focused on the bearing capacity, moment-curvature behavior and ductility properties of the samples. In addition, the relationship between the microcracks formed in the tensile regions of the samples and the stress amounts of the reinforcement was also investigated thanks to the FEA results. While the use of additives in the correct proportions used in GPC samples can increase the strength properties, excessive use of additives can reduce the strength of the samples. The load-displacement and moment-curvature behavior of

reinforced concrete samples varies depending on the strength properties and reinforcement ratios. In addition, the load-displacement behavior of the samples may vary depending on the experimental setups used and the loading speed. In the tension zone, fiber-reinforced concrete samples have higher ductility compared to OPC samples.

FEA results explain the relationships between the behaviors and findings of concrete samples in more detail. Thus, unpredictable behaviors and findings can be clarified by numerical analysis methods [14]. As a result of the tests conducted by Jinliang and Fangpu, the load capacity of concrete beams strengthened with CFRP with geopolymer adhesives increased and their flexural performance was better. As the number of CFRPs increased, the load capacity of the beams also increased. In the research, it was found that the majority of the tested beams broke under bending loads. In addition, the experimental results and the FEA analysis results support each other [15]. Differences in crack initiation, load-deformation characteristics and ultimate strength levels were revealed between GPC and OPC [16]. GPC exhibits superior flexural performance compared to OPC with higher bond strength, load capacity and ductility [13, 17]. While it is stated by Aziz et al. that GPC is more stable at high temperatures and has higher fracture energy, OPC has higher initial strength and durability properties [13]. In the study conducted by Wibowo et al. it can be said that GPC starts with linear elastic behavior in the moment-curvature response, as in reinforced concrete beams, and steel reinforcement becomes effective to provide moment transfer after cracking. However, the cracking behavior of GPC differs from that observed in OPC, so the moment-curvature response may also differ slightly [18]. According to Mortar et al. the stress distribution of GPC is more uniform and has more strength than OPC. In addition, GPC exhibits higher early strength and less cracking than OPC. The behavior of GPC under blast loads is better than OPC and more resistant to blasts [19]. It was stated that the shear strength of GPC beams is significantly higher than OPC beams in the study by Alex et al. It was stated that the difference between the splitting strengths of GPC and OPC beams was less, but GPC beams performed better in this property. It was also stated that GPC showed greater deformation than OPC at the same load level and that crack propagation was less. However, it was revealed that the deformations in the plastic region were greater in GPC beams than in OPC beams [20].

The experimental and numerical investigation of the structural behavior of geopolymer beams, the determination of design parameters, and the presentation of their advantages and disadvantages compared to OPC concrete are essential. These studies will facilitate and promote the use of GPC in structural design and construction sites. Comparing GPC beams with OPC beams and examining their compatibility with existing standards will help define their structural properties under challenging conditions. As a result, geopolymer concrete may emerge as a more reliable material in the construction industry.

Determining the behavior of steel-reinforced GPC beams will contribute to improving the design and construction processes of structures built with this material. While previous studies have investigated the structural behavior of beams with slag and fly ash additives, research on low-calcium fly ash-based GPC beams remains limited. Some experimental studies have kept the alkaline activator ratio constant, focusing on variables such as reinforcement ratio and curing temperature. However, this study considers alkaline activator ratio, curing method, and reinforcement ratios as variable parameters, providing a more comprehensive evaluation.

The variation in alkaline activator mixture ratios and curing techniques significantly affects the thermal, mechanical, and microstructural properties of GPC [4,6,21]. Therefore, determining the optimum values of these parameters and understanding their effects on structural behavior is of great importance. Furthermore, assessing the influence of reinforcement ratio on GPC beam performance is crucial for design optimization. In this context, 12 GPC and 3 OPC reinforced concrete beams were tested and analyzed using both experimental and numerical methods.

The aim of this study is to contribute to the practical, fast, and reliable design of GPC beams through FEA by comparing the finite element model results with experimental bending test data. Additionally, another objective is to determine the advantages and disadvantages of GPC compared to OPC. Numerical results obtained from FEM analysis and experimental findings were compared in terms of load-displacement and moment-curvature relationships. The numerical models developed based on experimental deformation data showed consistency with test results. Through FEA analyses, stress and scalar stiffness degradation (SDEG) behaviors were examined in detail, allowing for a more comprehensive interpretation of experimental data. As a result of these studies, FE models of GPC members were validated with experimental data, and recommendations for section design using numerical models were provided. This research aims to establish practical design guidelines and support the wider adoption of GPC members in the construction industry.

2. Material and method

2.1. Material properties

Class F fly ash, compliant with ASTM C618 and having a density of 2.32 g/cm^3, was utilized for the production of geopolymer concrete [22,23]. In Class F fly ashes, the combined proportion of chemical constituents such as SiO_2, Al_2O_3, and Fe_2O_3 (85.9 %) must be above 70 % of the total composition. The alkali activation of the fly ash in geopolymer concrete was performed using 14M NaOH

Table 1
Components of geopolymer concrete (kg/m^3).

Sample No	Sample Name	FA	SS	SH	SS/SH	AA/FA	Fine Aggregate	Coarse Aggregate
1	F1	406	122	81	1.5	0.5	643	1194
2	F2	406	158	45	3.5	0.5	643	1194

FA: Fly Ash, SS: Sodium Silicate Solution (Na_2SiO_3), SH: Sodium Hydroxide Solution (NaOH), AA: Sum of SS and SH.

and Na_2SiO_3 solutions. Crushed stone with a particle size range of 7–14 mm and a density of 2.6 g/cm^3 served as the coarse aggregate. Fine aggregate was provided by river sand with a particle size ranging from 0.1 to 4 mm and a density of 1.8 g/cm^3. Both types of aggregates were used in a saturated surface-dry condition without adding any water to the mix. During the beam fabrication process, two different formulations were used, varying solely in the ratio of the activation solutions (SS/SH) (Table 1).

In prior studies, it has been observed that the SS/SH ratio in geopolymer concretes typically ranges from 1.5 to 3.5 [24–26]. This research adopted the lower boundary (F1: SS/SH = 1.5) and upper boundary (F2: SS/SH = 3.5) from existing literature to ensure the study's scope was as comprehensive as possible. While other studies have reported that an SS/SH ratio of 2.5 and an AA/FA ratio of 0.5 resulted in the highest strength outcomes [4,27], the focus of this research is on both the structural behavior and strength of geopolymer reinforced concrete beams. Consequently, extreme SS/SH ratios were selected to explore these aspects in depth. Even if these ratios lead to lower strength, they allow for a broader comparison with traditional reinforced concrete beams, especially in terms of meeting reinforced concrete design standards and specifications.

2.2. Experimental study

In the study, FEM analyses of 3 OPC-RC beams and 12 GPC-RC beams, which were subjected to tests, were performed, and the results were compared. The variable test parameters for reinforced concrete beams were determined as the SS/SH ratio, curing method, and tensile reinforcement ratio. In experimental studies, GPC concrete was produced with SS/SH ratios of 1.5 and 3.5, and alkali activator solutions/fly ash (AA/FA) ratios of 0.5. The samples produced in these ratios were subjected to thermal curing at 90°C in an electric oven for 24 h. Thermal cure was applied to some samples immediately after manufacturing, and to the other samples after they were kept at ambient temperature for four days. In addition, 3 additional OPC beams were produced in order to determine the advantages and disadvantages of GPC concrete and to make comparisons. After the samples were kept for 28 days, four-point bending tests were performed in the laboratory (Fig. 1).

The stress-strain curves obtained from the cylindrical samples taken during the manufacturing of the samples and the splitting tensile test result data were used for the numerical study. Bending tests of GPC beam samples were conducted and finite element analyses were performed. The dimensions of the bending test beam were 150 x 300 × 3300 mm. The distance between the supports of simply supported beams was set as 3000 mm. The distance between the loading points was 900 mm.

Three different tensile reinforcement ratios were considered in the samples. The net cover was determined as 25 mm. The size and reinforcement details of the beam samples are shown in Fig. 2 and Table 2. The tensile reinforcement ratio in the beams were selected in accordance with the minimum (GB1), balanced (GB2) and maximum (GB3) limits according to the specification [23,28].

B420C steel reinforcement was used in experimental studies. The yield and tensile strengths obtained from tensile tests for this reinforcement class were used as numerical study parameters. The stress and strain curves of the reinforcement steel used in the FEM analysis are given in Fig. 9.

2.3. Analytical study

The models of OPC and GPC beam samples were presented in an analytical approach using the ABAQUS [29] program. The ABAQUS program is widely preferred for finite element analysis of reinforced concrete elements [30,31]. Dynamic Explicit analysis method was used for nonlinear analysis in the ABAQUS program. The SI unit system was used for modeling and analysis processes. Elastic and plastic behaviors were considered for creating material models. The CDP material model, known as Concrete Damaged

Fig. 1. Beam samples and experimental setup.

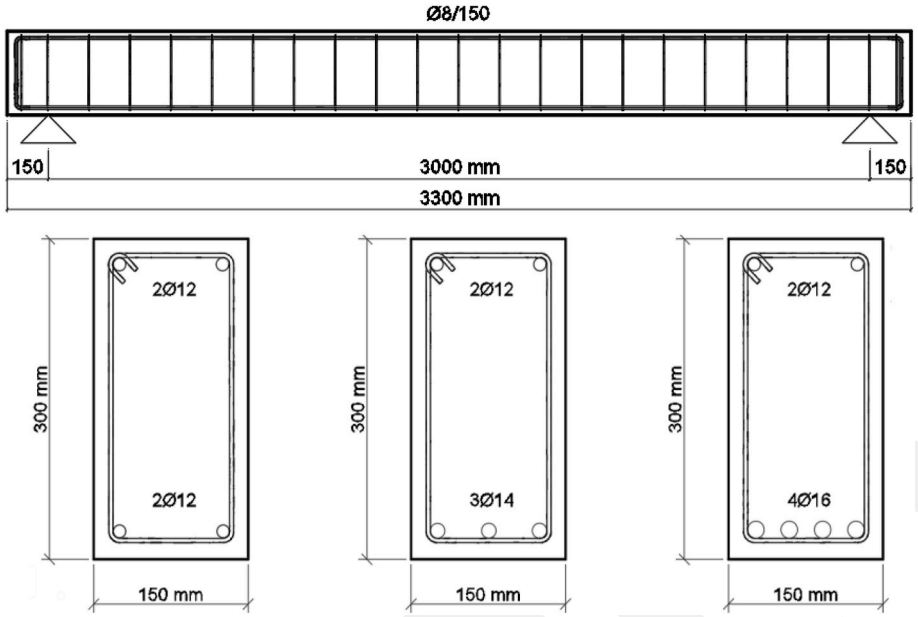

Fig. 2. Beam geometry and reinforcement details.

Table 2
Beam details.

No	Sample Name	Beam Size (mm)	Tensile Reinforcement	Reinforcement Ratio	SS/SH	Curing Start
1	OPCB1	150x300x3300	2 Ø 12	0.005	–	–
2	OPCB2	150x300x3300	3 Ø 14	0.010	–	–
3	OPCB3	150x300x3300	4 Ø 16	0.018	–	–
4	GB1F1C0	150x300x3300	2 Ø 12	0.005	1.5	Immediately
5	GB2F1C0	150x300x3300	3 Ø 14	0.010	1.5	Immediately
6	GB3F1C0	150x300x3300	4 Ø 16	0.018	1.5	Immediately
7	GB1F2C0	150x300x3300	2 Ø 12	0.005	3.5	Immediately
8	GB2F2C0	150x300x3300	3 Ø 14	0.010	3.5	Immediately
9	GB3F2C0	150x300x3300	4 Ø 16	0.018	3.5	Immediately
10	GB1F1C4	150x300x3300	2 Ø 12	0.005	1.5	+4 days
11	GB2F1C4	150x300x3300	3 Ø 14	0.010	1.5	+4 days
12	GB3F1C4	150x300x3300	4 Ø 16	0.018	1.5	+4 days
13	GB1F2C4	150x300x3300	2 Ø 12	0.005	3.5	+4 days
14	GB2F2C4	150x300x3300	3 Ø 14	0.010	3.5	+4 days
15	GB3F2C4	150x300x3300	4 Ø 16	0.018	3.5	+4 days

Tensile reinforcement (GB1: 2 Ø 12, GB2: 3 Ø 14, GB3: 4 Ø 16), SS/SH ratio (F1: 1.5, F2: 3.5), Curing start (C0: Direct, C4: After 4 days).

Plasticity, was used for concrete. To reveal the plastic behavior of concrete, the CDP model combines isotropic tensile and compressive plasticity, while using the concept of isotropic damaged elasticity [32–35]. The parameters of the CDP model were obtained from the results of the compression and splitting tensile tests of cylindrical samples used in beam production in the laboratory. The stress-strain curves obtained from the compression tests performed on the cylindrical samples were arranged for the CDP model and defined in the program. Material models were defined separately for different mixing ratios.

Series with SS/SH ratio of 1.5 and 3.5 were used. Thermal curing types, immediate and 4-day curing criteria, were considered for each series. In total, four different material models were created for GPC beams and one material model was created for OPC. CDP

Table 3
CDP parameters for ABAQUS material definition of concrete.

Parameter	Taken value	Description
f_{b0}/f_{c0}	1.16	The ratio of initial equibiaxial compressive yield stress to initial uniaxial compressive yield stress.
K	0.6667	K_c, the ratio of the second stress invariant on the tensile meridian
φ	30	Dilation angle
υ	0.0001	Viscosity parameter
ϵ	0.1	Eccentricity

model is used to define the damage mechanisms and crack development of concrete under load with a more realistic approach. Some parameters used for CDP model are given in Table 3. A total of 12 beam finite element models were created with two different SS/SH ratios, two different curing types and three different tensile reinforcement arrangements. In addition, three OPC beam models with three different tensile reinforcement arrangements produced by OPC were presented for comparison. The unit volume weight of concrete was calculated as 2.43 g/cm^3 for GPC samples and 2.4 g/cm^3 for OPC samples and entered into the program. f_{b0}/f_{c0} is the ratio of biaxial compressive strength to uniaxial compressive strength and its default value is 1.16 in ABAQUS program. The K value is used to define the ratio of the second stress invariant of compression and tension under the effect of similar hydrostatic stress. The viscosity parameter υ should preferably be at values close to 0 and allow the stresses to go beyond the yield surface [36,37]. The φ parameter is determined by sensitivity analysis and is the dilatation angle measured in the p-q plane under the effect of high pressure [38,39]. The ϵ parameter defines the speed at which the function approaches the asymptote and expresses the eccentricity.

For the values presented in Table 3 within the scope of finite elements, studies in the literature were taken as reference. All parameters were tested parametrically in the ABAQUS program. Considering the studies in the literature, many numerical modeling was analyzed and the most suitable values were obtained within the scope of geopolymer concrete [5,40–42].

2.3.1. Material models

The material model made use of the stress-strain curves that were acquired from the compression experiments conducted on each sample. The software tool was used to enter the yield and ultimate strengths of each sample, along with the corresponding plastic deformation values under these strengths. Each type of sample had its own elastic modulus value, which was computed and entered into the software program. Definitions of the CDP model were created within the parameters of the concrete model. The concrete's compressive behavior is seen in Fig. 3 [43].

In ABAQUS, variables like yield stresses and the inelastic unit strain values that follow from these stresses are entered to determine the compressive behavior of concrete. The graph's inelastic behavior relates to the section that comes after the yield stress and deformation values. Equation (1) [44] was used to get the values of inelastic strain, and Equation (2) was used to compute the values of stress.

$$\varepsilon_c^{in} = \varepsilon_c - \frac{\sigma_c}{E_0} \tag{1}$$

$$\sigma_c = (1 - d_c).E_0.\left(\varepsilon_c - \varepsilon_c^{pl}\right) \tag{2}$$

The software then calculates the plastic strain values after the inelastic strain values have been calculated and entered. Equation (3) is used to derive plastic strains. The damage characteristic unique to concrete under compressive loading is represented by the symbol d_c in Equation (4). This parameter indicates the reduction in elastic stiffness that occurs from loading beyond the graph's peak stress. This damage parameter is critical to accurately representing concrete's plastic behavior in the software and closely mimicking reality. Equation (4) was utilized to determine the outcome [44].

$$\varepsilon_c^{pl} = \varepsilon_c^{in} - \frac{d_c}{(1 - d_c)} \frac{\sigma_c}{E_0} \tag{3}$$

$$d_c = 1 - \frac{\sigma_c / E_0}{\sigma_c / E_0 + \varepsilon_c^{in}(1 - b_c)} \tag{4}$$

The ratio of plastic strain to inelastic strain is represented by the parameter b_c in the equation. Based on recent research, it was shown that the value for concrete falls between 0.5 and 0.7. [45,46]. The stress-strain (σ_t - ε_t) behavior shows elastic behavior under tensile axial loading, up to the maximum tensile stress (σ_{t0} - f_{ctk}) (Fig. 3). By dividing the greatest stress by the starting modulus of elasticity (E_0), one may determine the unit strain value, or ε_{t0}, that corresponds to σ_{t0}. Fig. 4 shows the tensile behavior of concrete

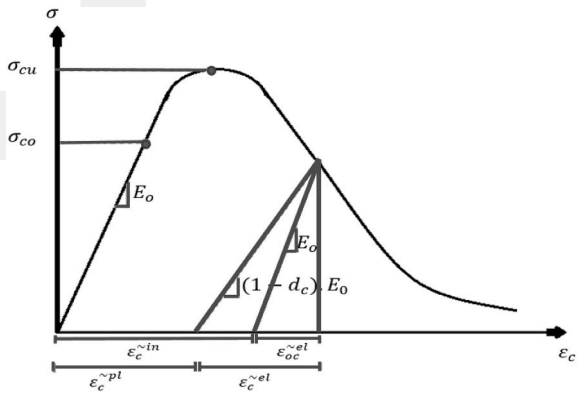

Fig. 3. Post-cracking compressive behavior of concrete.

[43].

Fig. 5 shows models for concrete tensile stiffness that are linear, bilinear, and exponential. [47]. Crack width is represented by the term w in the graph.

When modeling the tensile behavior of concrete, the post-cracking behavior of the concrete should be defined in the ABAQUS program. According to the material model defined in the program, the stress values (σ_t) of the concrete under the tensile effect are calculated according to Equation (5), and the plastic strain values ε_t^{pl} are calculated according to Equation (6) [43].

$$\sigma_t = (1 - d_t).E_0.\left(\varepsilon_t - \varepsilon_t^{pl}\right) \tag{5}$$

$$\varepsilon_t^{pl} = \varepsilon_t^{ck} - \frac{d_t}{(1 - d_t)} \frac{\sigma_t}{E_0} \tag{6}$$

The damage parameter of concrete under tensile effect is expressed as d_t and is calculated according to Equation (7). The expression ε_t^{ck} is the inelastic strain value after cracking and is calculated according to Equation (8) [44,48]. The expression b_t is a parameter included in the equations and takes a value between 0.1 and 0.7 in the literature [44,45].

$$d_t = 1 - \frac{\sigma_{t0}/E_0}{\sigma_{t0}/E_0 + \varepsilon_t^{ck}(1 - b_t)} \tag{7}$$

$$\varepsilon_t^{ck} = \varepsilon_t - \frac{\sigma_{t0}}{E_0} \tag{8}$$

Material properties of the compressive and tensile behavior of concrete were calculated for all different material models. Compressive behavior graphs and damage graphs were plotted with the data obtained from the compression tests. Tensile behavior graphs and damage graphs were plotted with the data obtained from the splitting tensile tests. The compression and damage behavior graphs of GPC concrete, which were drawn based on the cylinder specimen test results and the formulas above, are shown in Fig. 6. The tensile and damage behavior graphs of GPC concrete are shown in Fig. 7. The compression and tensile damage behavior graphs of OPC concrete are as in Fig. 8.

The stress-strain curve of the reinforcement obtained from the tensile tests in the study was also arranged by considering the CDP model and defined as data to the program [49,50]. The stress-plastic strain curves of these defined reinforcement types are given in Fig. 9. The program defined 200000 MPa for the elasticity modulus of the reinforcement and 0.3 for the poisson value. The material properties of the GPC and OPC samples are given in Table 4.

2.3.2. *Meshing*

Meshing and element type definitions were made for all material types. Compared to the reinforcements for the concrete beam section, the mesh size was larger, while the mesh size was smaller for compression, tension and transverse reinforcement. Using a 3D modeling tool, a concrete beam section simulation model was created using eight-node hexahedral elements (C3D8R) with reduced integration that can undergo deformation. Cubic finite elements were used for the analysis of the beams. T3D2 was used for the reinforcement and is a model consisting of 3D bar finite elements with two nodes and one degree of freedom. A parametric study was carried out to determine the ideal mesh size of the concrete. As suggested in the literature, 25, 30, 40 and 50 mm mesh tests were conducted in a cubic form with an aspect ratio of 1. The optimum mesh size for concrete was found to be 25 mm after mesh sensitivity study. The optimum mesh size for reinforcement was determined as 25 mm. The support and loading plates were similarly meshed as 25 mm. In this way, the bond length during the analysis was the same as the length formed in the test samples. Model and mesh views are shown in Fig. 10.

2.3.2.1. Mesh sensitivity. Element types are defined for all materials in mesh assignments. All materials were assigned to 3D, and the

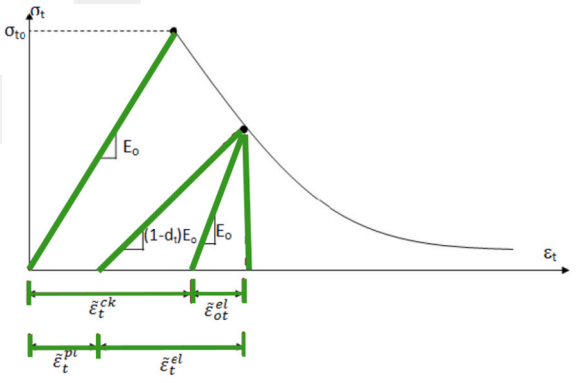

Fig. 4. Tensile behavior of concrete.

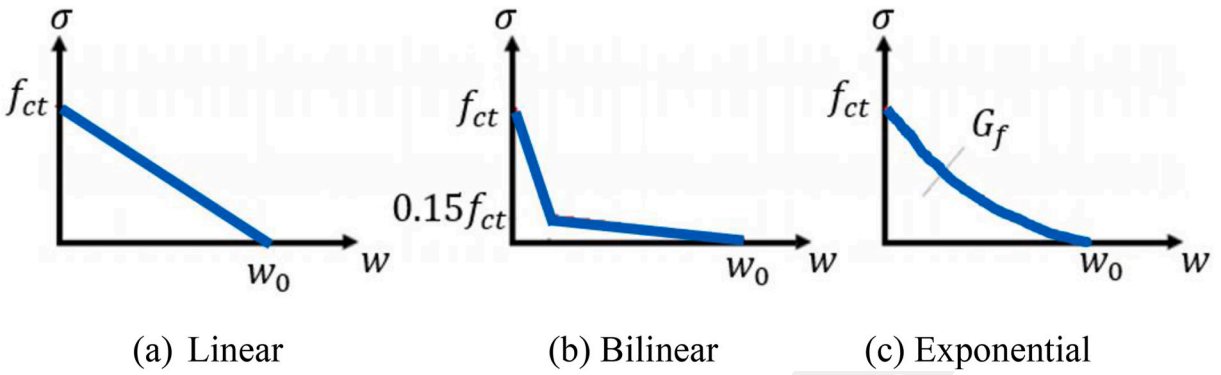

Fig. 5. Post-cracking tensile behavior of concrete.

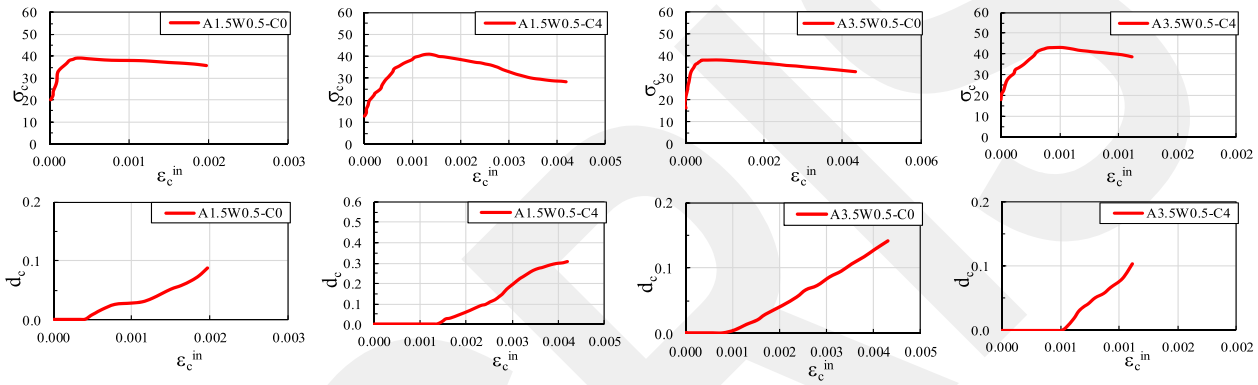

Fig. 6. Compressive-damage behavior graphs of GPC samples in numerical model.

beam was modeled as C3D8R. C3D8R refers to modeling with 8 nodes and 1 reduced integration point with 3 displacement degrees of freedom. The beam is solved as a cubic finite element. Loading and support plates are resolved with the same properties as the beam but with a higher mesh size. The reinforcements were analyzed as T3D2, that is, a 2-node 3D rod finite element with a single degree of freedom. Analyses were made by changing the mesh sizes of the relevant sample as fine, medium, and coarse. The mesh sizes of the relevant samples are presented in Table 5. Various mesh sizes were employed in the analysis for both rebar and concrete. The load-displacement curves obtained according to the analysis results according to mesh sizes are given in Fig. 11.

When the load-displacement curves are compared, decreasing the mesh size causes a decrease in the load value. For the GB1F1C0 sample, the 25 mm mesh size is the mesh size that is most compatible with the experimental results. As a result of the analyses, the 25 × 25 mm mesh size was determined in the reinforcement, while the 25 × 25 mm mesh size was determined in the sample concrete. As a consequence of the analyses made for all other GPC and OPC samples, the most suitable mesh size was determined to be 25 mm and was applied in this way.

2.3.3. Interactions and boundary conditions

In order to define the interaction between concrete and reinforcement in the numerical model, the embedded reinforcement model, which fully considers the adhesion between the two materials, was preferred. In the numerical model, the degrees of freedom of the embedded element are directly connected to the element (host region) in which it is embedded, and it is assumed that these elements move together during the analysis. The contact surfaces between the sample and the load and support plates are defined and connected to each other with the "tie constraint" in the numerical model. In the tie boundary condition, the degrees of freedom of the contact surfaces are numerically connected to each other, allowing the surfaces to move together.

2.3.4. Loading and analysis method

Four-point loading test was preferred for the study. The distance between the loading points was determined as 900 mm. Displacement demand was applied to the loading points. Target displacement value was determined and amplitude values were entered in accordance with the analysis method and duration. Structural reactions and behaviors corresponding to this target displacement were analyzed. Load values were obtained from the support points and load-displacement curves were plotted under these loadings. The analysis was performed according to the Dynamic/Explicit method in the study. The Explicit method is generally used in cases where advanced damage occurs in impact events or collapse mechanisms. The reason why open methods are more

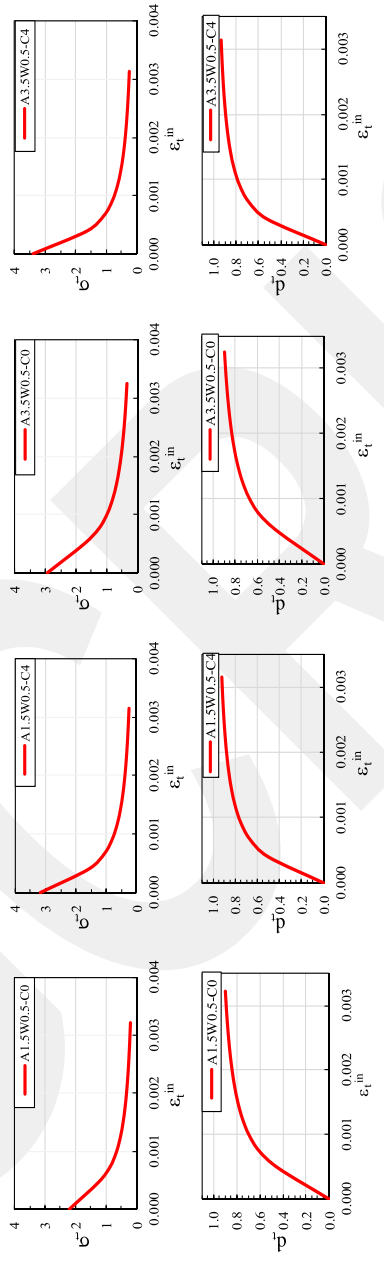

Fig. 7. Tension-damage behavior graphs of GPC samples in numerical model.

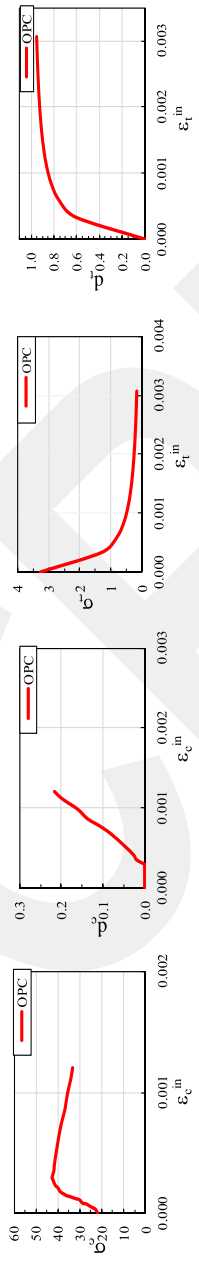

Fig. 8. Compressive and tension damage behavior graphs of OPC samples in numerical model.

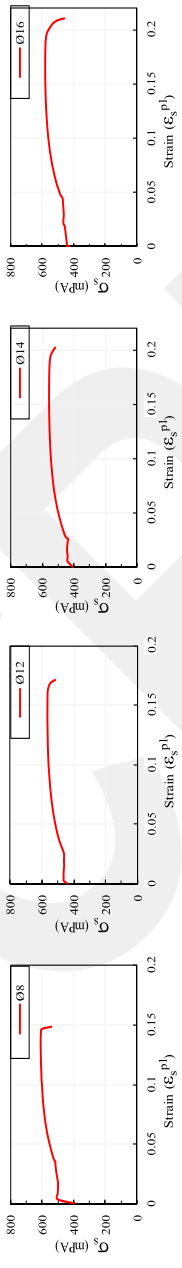

Fig. 9. Rebars stress-plastic strain curve.

Table 4
Material properties of GPC and OPC concrete.

Sample Name	f_c (MPa)	f_t (MPa)	E_c (MPa)	Poisson's Ratio
A1.5W0.5-C0	39.00	2.22	14067	0.20
A1.5W0.5-C4	41.21	3.17	19978	0.20
A3.5W0.5-C0	38.49	2.94	16714	0.20
A3.5W0.5-C4	43.09	3.40	23014	0.20
OPC	42.47	3.25	21022	0.18

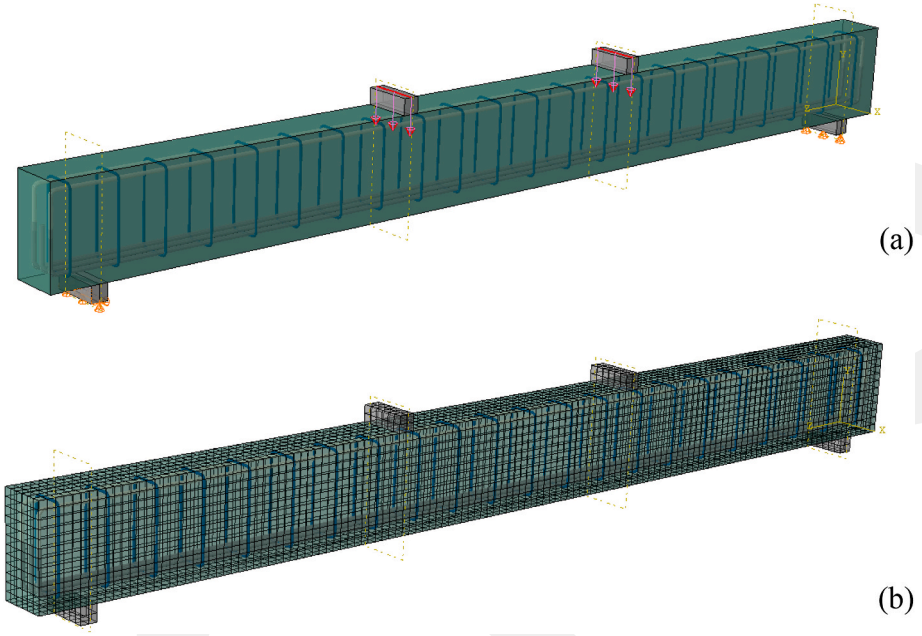

Fig. 10. The schematic views of modeling details ((a) Model, support and loading views, (b) Mesh views).

Table 5
Mesh sizes of samples.

Sample Name	Rebar Mesh Size (mm)	Concrete Mesh Size (mm)
GB1F1C0	25 × 25	25 × 25
GB1F1C0-1	20 × 20	20 × 20
GB1F1C0-2	30 × 30	30 × 30
GB1F1C0-3	40 × 40	40 × 40
GB1F1C0-4	50 × 50	50 × 50

suitable for the study is that material damping and inertia effects are included in the analysis.

2.3.5. Limitations of experimental and FEM methods

Both experimental and numerical methods have inherent limitations that influence result accuracy and applicability. Experimental studies are affected by laboratory conditions, material variability, and measurement precision, while FEM analyses rely on modeling assumptions, boundary condition idealizations, and numerical stability. These factors contribute to the discrepancies observed between the two approaches, particularly in load-displacement and moment-curvature responses.

The limitations of the experimental setup and FEM analysis used in this study are summarized in Table 6. Experimental constraints primarily stem from environmental factors, test setup, and measurement accuracy, whereas FEM limitations arise from material modeling assumptions, mesh sensitivity, and idealized boundary conditions.

As shown in Table 6, experimental results are influenced by environmental conditions and test setup constraints, whereas FEM analyses depend on material modeling accuracy and numerical parameters. The observed differences in ultimate load and displacement values can largely be attributed to these limitations. While experimental validation enhances the reliability of FEM predictions, further refinements in material modeling, boundary conditions, and numerical strategies could improve the correlation between the two methods. Future studies may incorporate long-term loading effects, environmental exposure, and alternative modeling approaches

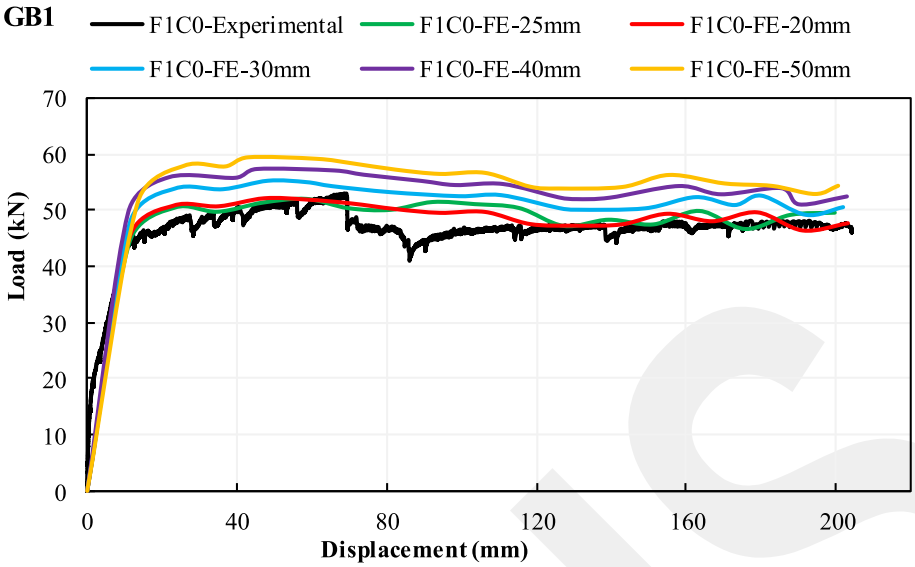

Fig. 11. Load-displacement curves of analyses of sample geopolymer concrete at different mesh sizes.

Table 6
Comparison of limitations in experimental and FEM methods.

Limitation Type	Experimental Limitations	FEM Limitations
Testing Conditions	Variations in temperature, humidity, and material properties affect consistency.	Assumes homogeneous and isotropic material behavior, neglecting local heterogeneities.
Measurement Accuracy	Sensor precision and human error introduce variability in displacement and strain readings.	Mesh size and element selection influence numerical accuracy and convergence.
Testing Scope	Limited to specific beam dimensions; real-scale behavior may differ.	Boundary conditions are simplified, potentially deviating from real structural constraints.
Material Behavior	Microstructural changes over time and localized defects are not fully captured.	Concrete-rebar interaction and damage evolution depend on model assumptions.
Load and Failure Mechanisms	Only bending behavior is assessed; shear and cyclic loading are not considered.	Crack propagation and failure patterns depend on mesh density and numerical assumptions.
Generalization to Real Structures	Results are specific to controlled lab conditions and may not directly translate to field applications.	Long-term effects such as creep, fatigue, and environmental degradation are not included.

to bridge the gap between numerical and experimental findings.

3. Results and discussion

In the study, the experimental results obtained by subjecting 12 heat-cured GPC beams and 3 OPC beams with 3 different reinforcement ratios to four-point bending tests were compared with the numerical results obtained by modeling and analyzing the same beams in the ABAQUS program.

3.1. Load-deflection curve

Beam samples with different reinforcement ratios were compared both within themselves and in terms of numerical and experimental results, and the load-displacement curves are given in Fig. 12. The code labeled FE from the beam samples with the same name shows the results obtained from the finite element analysis (FEA).

When the experimental and numerical graphs obtained from beams with minimum reinforcement (GB1) and balanced reinforcement ratio (GB2) are compared, it can be said that the load-deformation behaviors of all samples in the linear elastic region are quite close to each other and the numerical model successfully captures the experimental data. In the region where the beam samples leave the linear behavior and turn to nonlinear behavior, the load-displacement curves in GB1 beams are quite close to each other. It was observed that the load obtained from the numerical model was higher at the points where the graphs turned into nonlinear behavior in GB2 beams. In addition, the specific behavior of the GPC in this region, where it increases its strength a little by taking on the load again after the sudden load drop and continues to displace, was also observed in the graphs obtained from the finite element model. After the ultimate load was reached, it was seen that the agreement between the numerical and experimental data was preserved in GB1 beams in all graphs. However, the point where the ultimate load is reached has reached a higher value in the graphs

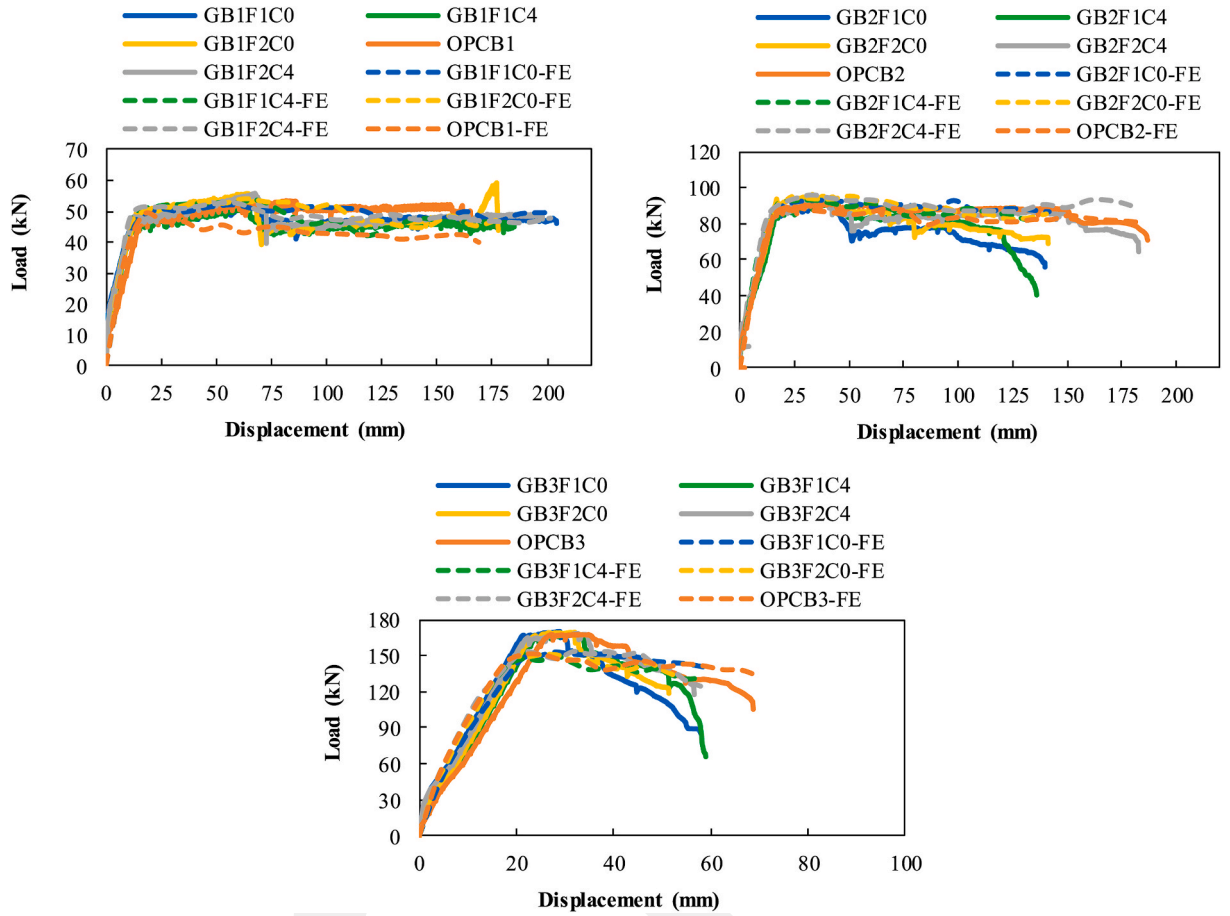

Fig. 12. Comparison of experimental and numerical load-displacement curves according to reinforcement ratios.

drawn with numerical data in GB2 beams. In the comparison made for OPC graphs, it was seen that the experimental and numerical results were almost the same in the elastic region, but some differences were observed in the region where nonlinear behavior was dominant, and also a slight load drop was experienced in the numerical results but recovered afterwards. The samples that best reflect the unique low elasticity and high deformation behavior of GPC were the samples that were cured with heat after resting at room temperature for 4 days in terms of curing method. When the experimental and numerical data obtained from the beams with maximum tensile reinforcement ratio (GB3) were compared, some separation was observed in the curves compared to GB1 and GB2 beams from the point where the first crack was observed. This situation is observed in experimental data and is also reflected in the graphs obtained from the numerical data. When the ultimate loads and displacements of the GB3 beams are investigated, the values of the curves obtained from the experimental data are higher and the numerical model used in the FE analysis makes lower predictions.

The critical points obtained from the experimental and numerical studies of GPC and OPC beam specimens are given in Table 7. The load at which the first crack occurs and the corresponding displacement are expressed as the yield load and the corresponding displacement, which is the point at which the reinforcement yields, and the ultimate load and the corresponding displacement, which is the load at which the compression zone of the concrete is crushed. As seen from Table 7, at the point where the first crack occurs in the minimum reinforced GPC-GB1 beam specimens, the numerical displacement values are around 1.8 to 3.5 times the experimental displacement values, while the load values are around 0.8–1.2 % times. At the yield point, the difference between the load and displacement obtained from the experimental and numerical results are quite close to each other. The difference between the data is approximately 3 % for the load and 20 % for the displacement. At the ultimate point, the difference is approximately 6 % for the load and 12 % for the displacement values. According to the experimental and numerical data, the difference for the displacements of the OPC sample is 13 % at the first crack point, 9 % at the yield point and 17 % at the ultimate point, respectively. The difference between the load values is 15 % at the first crack point, 4 % at the yield point and 14 % at the ultimate point. When GPC-GB2 beams with balanced reinforcement ratio are investigated according to Table 7; the average displacement at the first crack point between experimental and numerical data are 1.75–2.5 times. The difference between the loads at the same point is 1.1–1.5 times. At the yield point, the difference between the displacements is 5 % on average, while the difference between the loads is 3 % on average. At the ultimate load point, the displacement difference is 15 % on average and the load difference is 1 %. For the displacements of the OPC sample, the numerical data at the first crack point is 2.19 times bigger than the experimental data. The difference at the yield point is 1

Table 7
Critical values of load-displacement graphs of GPC and OPC beam test and FE samples.

Sample Name	GB1						GB2						GB3					
	First Crack Point (Load Controlled)		*Yield Point (Disp. Controlled)*		*Ultimate Point (Crushed)*		*First Crack Point (Load Controlled)*		*Yield Point (Disp. Controlled)*		*Ultimate Point (Crushed)*		*First Crack Point (Load Controlled)*		*Yield Point (Disp. Controlled)*		*Ultimate Point (Crushed)*	
	Δ (mm)	*F (kN)*	*Δ (mm)*	*F (kN)*	*Δ (mm)*	*F (kN)*	*Δ (mm)*	*F (kN)*	*Δ (mm)*	*F (kN)*	*Δ (mm)*	*F (kN)*	*Δ (mm)*	*F (kN)*	*Δ (mm)*	*F (kN)*	*Δ (mm)*	*F (kN)*
F1C0	1.62	20.03	12.12	46.06	69.64	47.12	2.30	25.09	16.33	86.46	41.63	91.12	4.29	50.12	21.44	167.07	29.02	168.13
F1C0-FE	5.63	22.10	11.30	44.30	58.60	52.00	3.93	26.80	15.60	85.54	40.10	92.95	3.09	33.53	21.36	147.94	27.88	153.00
F1C4	1.44	15.37	12.61	45.73	65.91	48.19	2.39	23.16	16.98	86.99	44.63	90.26	4.30	40.06	24.02	164.87	32.26	167.67
F1C4-FE	2.82	11.80	11.20	47.30	57.90	52.80	4.20	31.61	16.93	90.28	42.13	91.36	3.10	40.19	18.28	141.95	24.84	146.03
F2C0	2.82	21.16	14.13	49.99	64.89	51.78	2.16	25.15	16.86	93.58	43.34	93.85	2.90	36.27	23.51	166.07	28.31	168.86
F2C0-FE	5.06	22.30	20.90	50.90	63.10	54.10	4.20	30.06	16.94	89.61	42.34	93.70	2.80	38.18	19.49	148.43	28.49	150.54
F2C4	1.94	19.96	14.22	46.99	69.04	52.25	1.97	25.02	17.45	86.93	40.66	92.32	2.54	40.0	21.98	164.01	34.79	165.00
F2C4-FE	5.33	24.30	11.30	48.63	58.30	52.70	5.04	36.69	15.04	88.14	61.00	93.10	3.10	41.34	21.50	153.23	31.84	153.60
OPC	3.73	15.10	18.68	46.93	86.36	51.92	1.79	20.16	15.56	85.00	44.83	87.79	2.04	20.03	27.18	167.47	35.52	165.74
OPC-FE	4.21	17.30	17.00	48.90	71.40	44.80	3.92	26.59	15.71	84.60	40.65	86.48	3.65	46.34	17.88	144.81	29.57	124.61

% and at the ultimate point is 9 %. The numerical data is 1.32 times greater than the experimental data in terms of loads. The difference at the yield point is 0.5 % and at the ultimate point is 1.5 %. Finally, the numerical displacements at the first crack point in the GPC-GB3 beams with maximum reinforcement are between 0.72 and 1.22 times larger than the experimental displacement data in Table 7. The load values are between 0.67 and 1.05 times. According to the results obtained from the numerical and experimental data, the difference between the displacement and load values at the yield point is 10 % on average. At the ultimate point, these values are 9 % and 10 % on average for displacement and load, respectively. For the displacements of the OPC sample, the numerical data at the first crack point is 1.79 times the experimental data, while the load value is 2.31 times. The difference at the yield point for load and displacement values is 13.53 % and 34.21 %, respectively. At the ultimate point, the displacement difference is 16.75 % and the load difference is 24.82.

When the above results are investigated, the best agreement between the experimental and numerical data was achieved in the GB1F2C0 sample for minimum reinforced beams, in the GB2F2C0 sample for balanced reinforced beams and in the GB3F2C4 sample for maximum reinforced beams. Accordingly, the samples with a SS/SH ratio of 3.5 provided the best results. In terms of curing technique, the samples immediately cured with heat in beams with minimum and balanced reinforcement are compatible, while in beams with maximum reinforcement, the analytical and numerical results of the samples cured with heat after resting for 4 days are compatible. The closest results in terms of load belong to beams with minimum reinforcement, while in terms of displacement, they belong to beams with maximum reinforcement.

3.2. Moment-curvature graph

The moment-curvature graphs drawn with the help of experimental data and the graphs obtained from the FEA are given in Fig. 13 according to the reinforcement ratios. In real applications, the last performance point that can be reached in terms of beam is the point where the concrete in the compression zone is crushed. For this reason, the experimental moment-curvature graphs were terminated at the moment when the concrete in the beam compression zone was crushed. Accordingly, the moment-curvature graphs obtained from the numerical data were also drawn in this way. The near-linear lines obtained from the numerical and experimental data in the elastic zone and up to the yield point in all the minimum, balanced and maximum reinforced GPC beams are compatible with each other.

However, the slope of the line of numerical data is lower in OPC beams. Numerical models created for minimum reinforced GPC-GB1 beams estimate the curvature value slightly underestimate. In OPC beams, unlike GPC samples, the curvature value of numerical models was calculated higher than the curvature value of experimental data. Similarly, the moment curvature graphs from the beginning of the test to the part where the first crack was observed and then to the part where the reinforcement yields are quite close to each other experimentally and numerically in GPC-GB2 beams with balanced reinforcement ratio. In balanced reinforced OPC beams, the slope was obtained lower in the part up to the yield moment. The curvature values calculated from the FEA were smaller at the end of the test. This also underestimated the curvature values of the numerical GPC beam models with balanced reinforcement. The most significant difference was observed between the linear graphs of numerical and experimental data in the section up to the yield moment in GPC-GB3 beams with maximum reinforcement ratio. Accordingly, the slope of numerical data is lower than that of the experimental. In all samples, the ultimate moment point and beyond were not captured. Therefore, in general, numerical models underestimated the curvature value at the breaking point. The greatest difference between the moment-curvature graph obtained from the FEA and the moment-curvature graphs drawn with experimental data was observed in the maximum reinforced GPC beams. The difference between the lines drawn up to the yield moment section of OPC beams, similar to that of GPC samples, is found mostly in beams with maximum reinforcement. However, the OPC graphs obtained from numerical and experimental data are also different from each other. In addition, the curvature obtained as a result of numerical analysis is greater than that obtained from experimental data, and the numerical OPC model overestimates the curvature values of beams with maximum reinforcement.

Some critical points obtained from experimental and numerical studies of GPC and OPC beam samples are presented in Fig. 14. These points are the cracked moment, which is the moment value at which the first crack appears in the beam section, the yield moment, which is the moment value at which the other point reinforcement yields, and the ultimate moment, which is the moment value at which the final point concrete compression zone is crushed. When the yield moment values in GB1 beams were compared, there was a difference of 1 %–5 % between the numerical and experimental results and that the models gave results very close to the experimental data. The difference between the ultimate moments was around 7 % on average. While the difference between the yield moments in GB2 beams was around 3 % on average, the average difference between the ultimate moments was around 6 %. In GB3 beams, the difference between yield moments is around 10 % on average, while the difference between ultimate moments is around 7 %. In general, the closest results obtained by GPC numerical models are obtained from yield moment estimation with a deviation of 5.53 %, followed by ultimate moment with a deviation of 6.51 %. In minimum and balanced reinforced GPC beams, the lowest deviation values are in samples with C0 curing technique, while in maximum reinforced sections, they are in samples with C4 curing technique. In OPC samples, the situation is similar to GPC samples, and the best estimates belong to yield and ultimate moments, respectively. However, the moment estimation performances of OPC numerical models are lower than those of GPC numerical models. In addition, OPC numerical models have lower estimations for ultimate moments than experimental data. The opposite is the case for GPC samples.

The deflections of GPC and OPC beams from numerical and experimental data are given in Fig. 15 for the first crack moment, yield point and ultimate point, which is the point where the concrete compression zone is crushed. Accordingly, the deflection amount at the first crack moment obtained from the numerical models for all beam sections was obtained as higher (overestimated) than the experimental data and the biggest difference occurred at this value. The average differences between yield deflections obtained from numerical and experimental data are 21.39 % for minimum reinforcement ratio, 4.79 % for balanced reinforcement ratio and 10.76 %

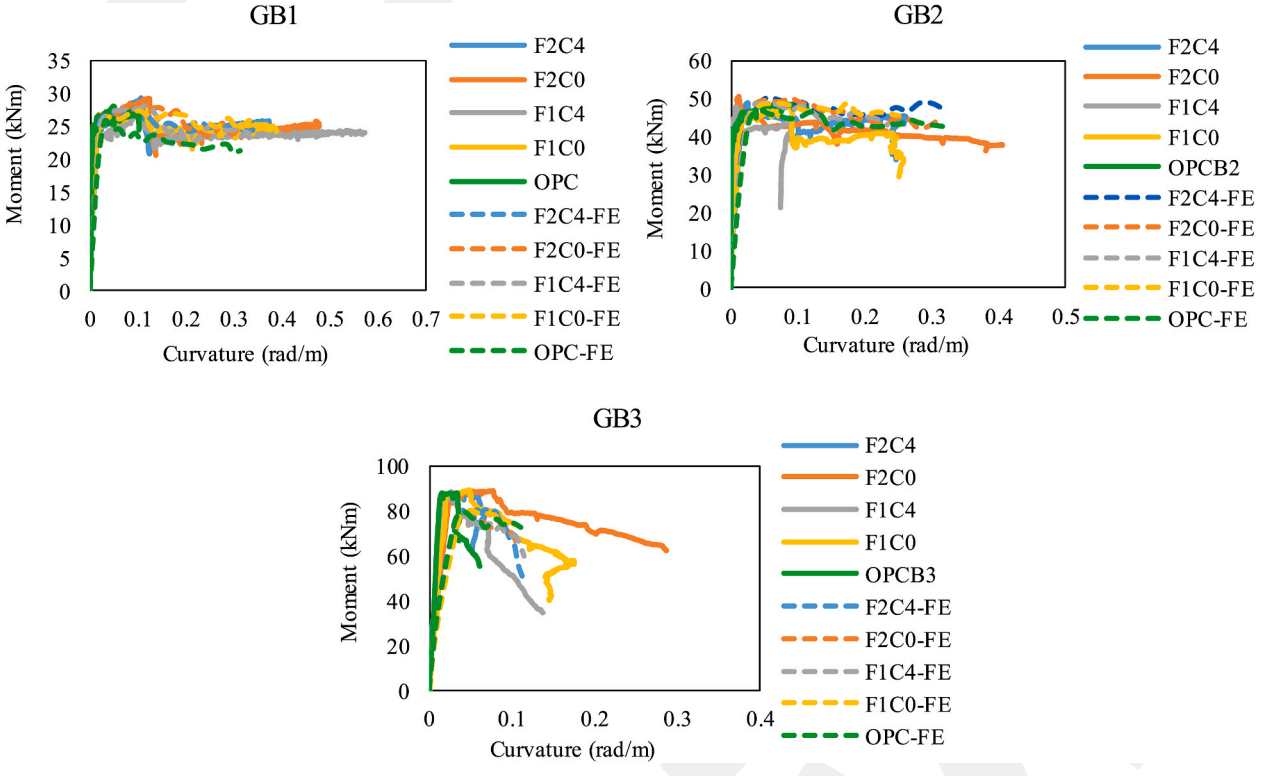

Fig. 13. Comparison of experimental and numerical moment-curvature graphs according to reinforcement ratios.

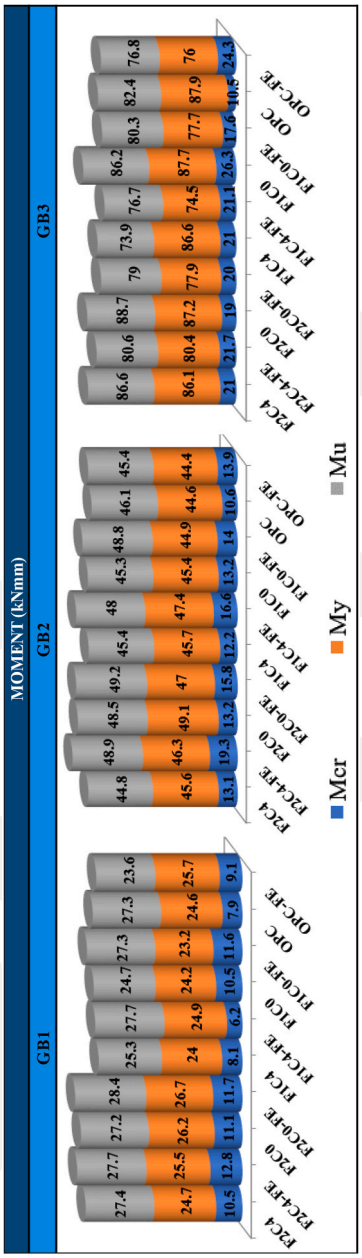

Fig. 14. Cracking moment, yield moment and ultimate moment of GPC and OPC beams (kNm).

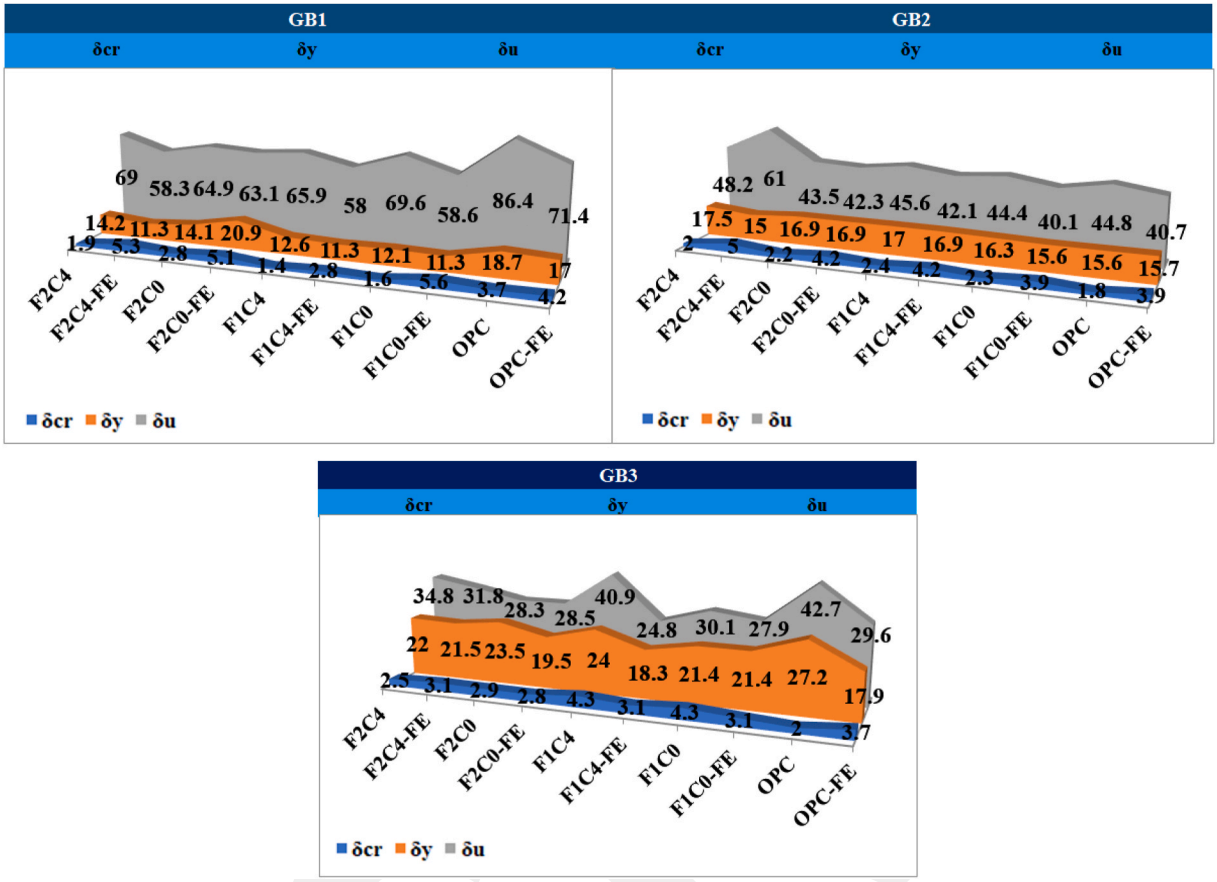

Fig. 15. Cracking, yielding and ultimate deflection values of GPC and OPC beams (mm).

for maximum reinforcement ratio, respectively. The average difference between ultimate deflection points was calculated as 11.51 % for minimum reinforced beams, 11.67 % for balanced reinforced beams and 14 % for maximum reinforced beams. In general, the deflection amounts calculated by the numerical models were below the experimental results. When all beam samples were considered, the difference between the average yield deflections was 12.32 %, while the difference between the ultimate deflections was 12.40 %. When the deflections for the beam samples at each reinforcement ratio were investigated, the closest values were obtained from the samples with maximum, balanced and minimum reinforcement ratios, respectively. The best results for OPC specimens were obtained from beams with minimum reinforcement ratio. Also, especially for yield and ultimate deflections, deflection approaches of OPC numerical models were behind GPC numerical models. The yield and ultimate deflection curves obtained from experimental and numerical data are graphically very similar to each other.

The observed differences between experimental and numerical results can be attributed to several factors, including material modeling assumptions, boundary condition idealizations, and the limitations inherent to both methods. While the experimental results reflect real material behavior, they are subject to environmental variations and measurement uncertainties. On the other hand, FEM provides controlled and repeatable simulations but relies on idealized assumptions regarding material homogeneity, mesh sensitivity, and damage progression. These factors collectively influence the deviations observed in load-displacement and moment-curvature responses.

Table 8
Experimental-numerical consistency analysis for GPC and OPC concrete.

Parameter	t-statistic (GPC)	p-value (GPC)	t-statistic (OPC)	p-value (OPC)
Ultimate Load	1.5305	0.1541	1.3302	0.3148
Ultimate Displacement	0.9784	0.3489	2.5057	0.1291
Yield Load	2.1105	0.0585	0.8961	0.4648
Yield Displacement	1.1246	0.2847	1.2476	0.3385
First Crack Load	−0.7303	0.4805	−1.5670	0.2576
First Crack Displacement	−3.0163	0.0117	−2.8882	0.1019

3.3. Statistical evaluation of numerical and experimental data

In this section, a statistical evaluation of the numerical and experimental results is presented to assess the accuracy and reliability of the developed models. The t-statistics and p-values for both Geopolymer Concrete (GPC) and Ordinary Portland Cement (OPC) concrete samples are summarized in Table 8, while Table 9 provides the standard deviation and confidence intervals for the numerical and experimental results.

The p-values indicate whether the numerical and experimental results exhibit statistically significant differences. Typically, a p-value below 0.05 suggests a significant discrepancy. It is observed that the first crack displacement exhibits a statistically significant difference for the GPC sample ($p = 0.0117$), indicating a notable deviation between numerical and experimental values. Other parameters, however, remain within an acceptable range, supporting the reliability of the numerical models.

According to the results obtained from the numerical and experimental data, the difference between the displacement and load values at the yield point is 10 % on average. At the ultimate point, these values are 9 % and 10 % on average for displacement and load, respectively. For the displacements of the OPC sample, the numerical data at the first crack point is 1.79 times the experimental data, while the load value is 2.31 times. The difference at the yield point for load and displacement values is 13.53 % and 34.21 %, respectively. At the ultimate point, the displacement difference is 16.75 % and the load difference is 24.82.

When the yield moment values in GB1 beams were compared, there was a difference of 1 %–5 % between the numerical and experimental results and that the models gave results very close to the experimental data. The difference between the ultimate moments was around 7 % on average. While the difference between the yield moments in GB2 beams was around 3 % on average, the average difference between the ultimate moments was around 6 %. In GB3 beams, the difference between yield moments is around 10 % on average, while the difference between ultimate moments is around 7 %. In general, the closest results obtained by GPC numerical models are obtained from yield moment estimation with a deviation of 5.53 %, followed by ultimate moment with a deviation of 6.51 %.

The average differences between yield deflections obtained from numerical and experimental data are 21.39 % for minimum reinforcement ratio, 4.79 % for balanced reinforcement ratio and 10.76 % for maximum reinforcement ratio, respectively. The average difference between ultimate deflection points was calculated as 11.51 % for minimum reinforced beams, 11.67 % for balanced reinforced beams and 14 % for maximum reinforced beams. In general, the deflection amounts calculated by the numerical models were below the experimental results. When all beam samples were considered, the difference between the average yield deflections was 12.32 %, while the difference between the ultimate deflections was 12.40 %.

3.4. Numerical stress and damage distributions

The compatibility of the numerical results with the experimental data is shown in the previous sections. In addition to the comparison of the experimental and numerical results, some structural behaviors that cannot be obtained experimentally can be obtained from the analysis results of the numerically created finite element models. In this context, SDEG graphs for stress and scalar stiffness degradation were obtained and the results were compared among themselves. Stress and SDEG graphs of the numerical results are shown in Figs. 16–30.

When the numerical stress and SDEG behaviors of GB1-GPC beams with 2 Ø 12 tensile reinforcement are investigated, there is no significant difference between GPC and OPC beams in terms of average stress at the yield point, but the damage conditions differ from each other. While the damages in GPC beams are local, OPC cracks are spread homogeneously on the surface. In the ultimate case, the stress values in the compression zone in GPC beams are on average 72 % larger than in OPC beams. While the damage becomes apparent locally between the loading points in GPC beams, the damage in OPC beams is again homogeneously distributed, this time combined with the compression zone. The reason for this situation is that the GPC elasticity modulus is low, and it shows that there is a larger deformation demand in order to reach similar strength in the compression zone with OPC. Since the compression zone is not damaged in GPC beams, it has less deflection in the ultimate state than OPC beams (Table 7). However, the compression zone did not

Table 9
Standard deviation and confidence intervals for experimental and numerical results.

Group	Mean (GPC)	Standard Deviation	Lower Confidence Limit	Upper Confidence Limit
GB1 - Ultimate Load	49.835	2.5621	45.7582	53.9118
GB1 - Ultimate Displacement	67.37	2.3255	63.6696	71.0704
GB1 - Yield Load	47.1925	1.9398	44.1058	50.2792
GB1 - Yield Displacement	13.27	1.0646	11.5760	14.9640
GB1 - First Crack Load	19.13	2.5663	15.0465	23.2135
GB1 - First Crack Displacement	1.955	0.6126	0.9802	2.9298
GB2 - Ultimate Load	91.8875	1.5574	89.4094	94.3656
GB2 - Ultimate Displacement	42.565	1.7671	39.7531	45.3769
GB2 - Yield Load	88.49	3.4016	83.0773	93.9027
GB2 - Yield Displacement	16.905	0.4602	16.1727	17.6373
GB3 - Ultimate Load	167.415	1.6829	164.7371	170.0929
GB3 - Ultimate Displacement	31.095	3.0040	26.3150	35.8750
GB3 - Yield Load	165.505	1.3425	163.3688	167.6412
GB3 - Yield Displacement	22.7375	1.2246	20.7889	24.6861

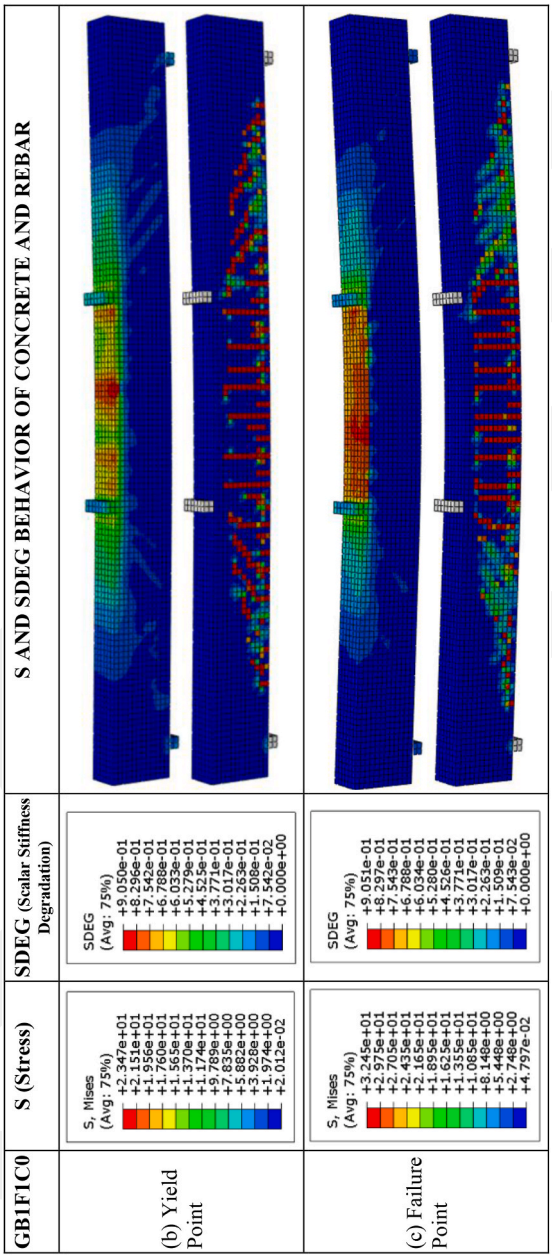

Fig. 16. Stress and SDEG graphs of the GB1F1C0 beam at yield and failure points.

Fig. 17. Stress and SDEG graphs of the GB1F1C4 beam at yield and failure points.

Fig. 18. Stress and SDEG graphs of the GB1F2C0 beam at yield and failure points.

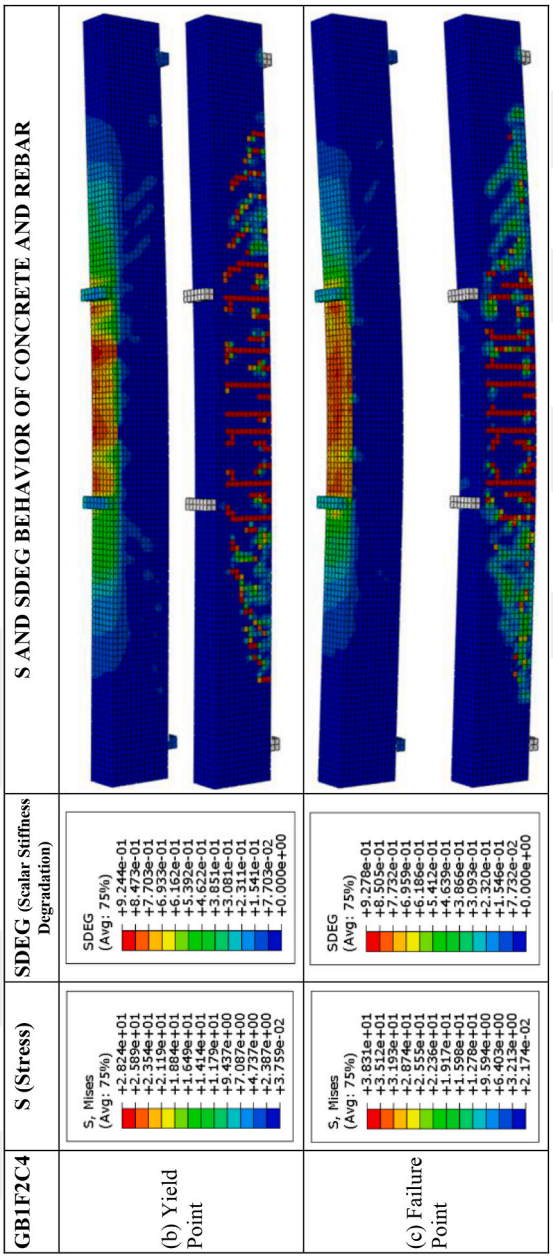

Fig. 19. Stress and SDEG graphs of the GB1F2C4 beam at yield and failure points.

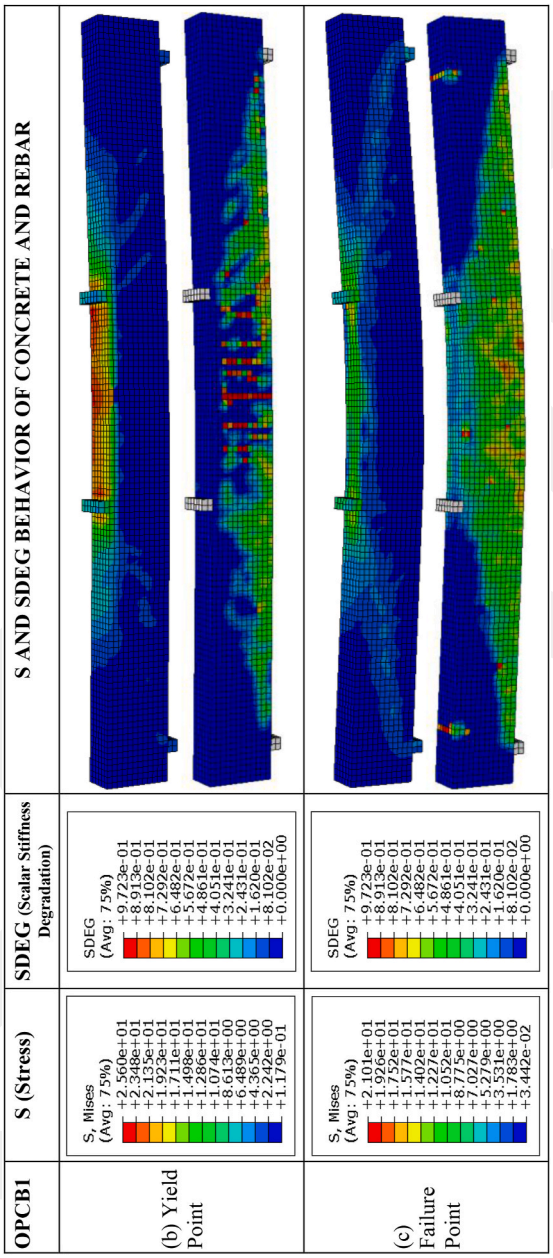

Fig. 20. Stress and SDEG graphs of OPCB1 beam at yield and failure point.

Fig. 21. Stress and SDEG graphs of the GB2F1C0 beam at yield and failure points.

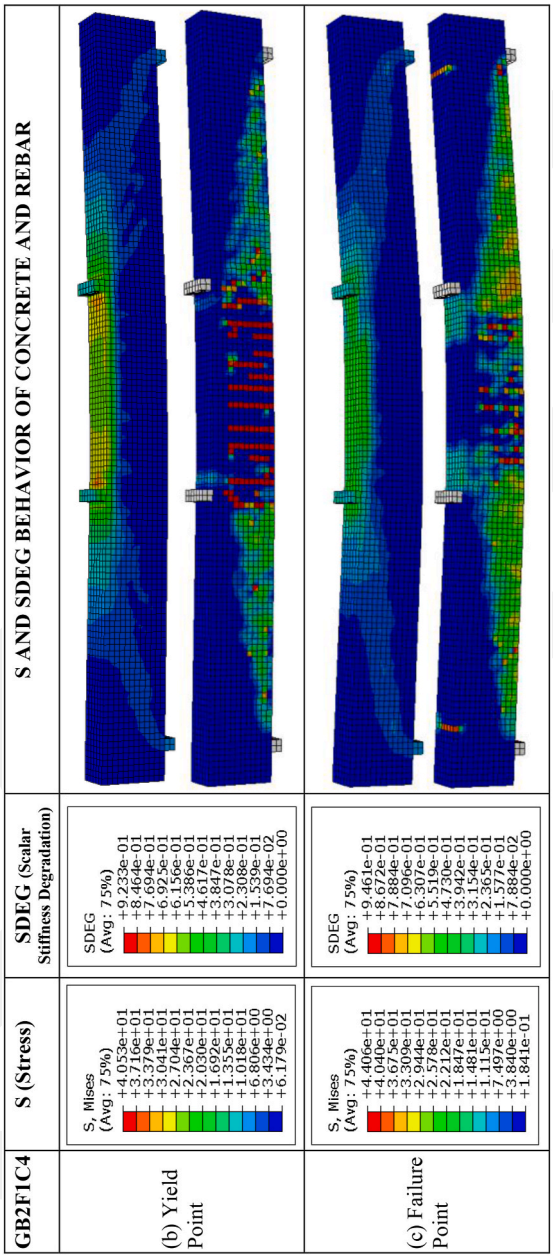

Fig. 22. Stress and SDEG graphs of the GB2F1C4 beam at yield and failure points.

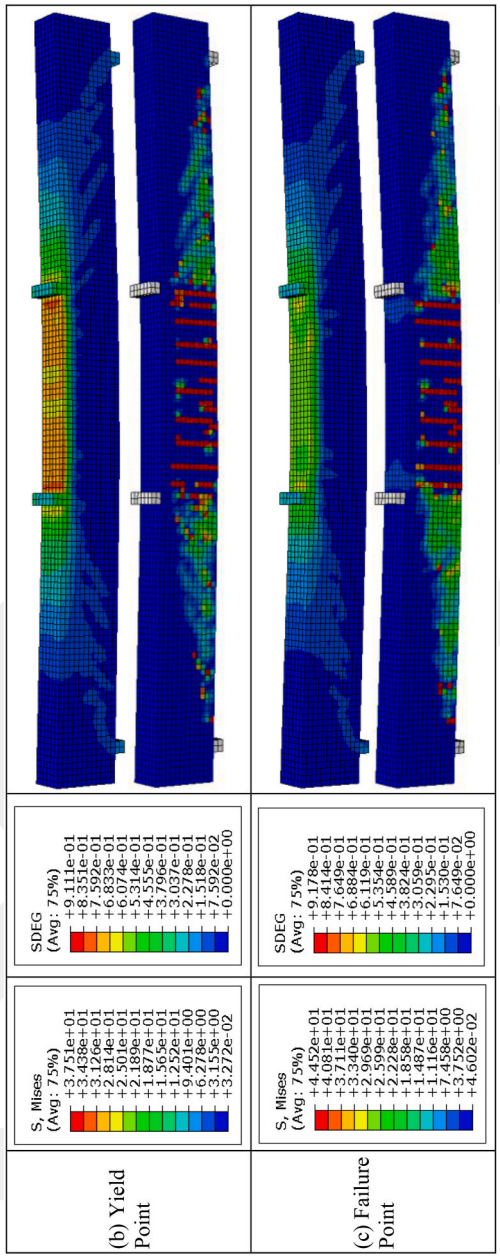

Fig. 23. Stress and SDEG graphs of the GB2F2C0 beam at yield and failure points.

Fig. 24. Stress and SDEG graphs of the GB2F2C4 beam at yield and failure points.

Fig. 25. Stress and SDEG graphs of OPCB2 beam at yield and failure point.

Fig. 26. Stress and SDEG graphs of the GB3F1C0 beam at yield and failure points.

Fig. 27. Stress and SDEG graphs of the GB3F1C4 beam at yield and failure points.

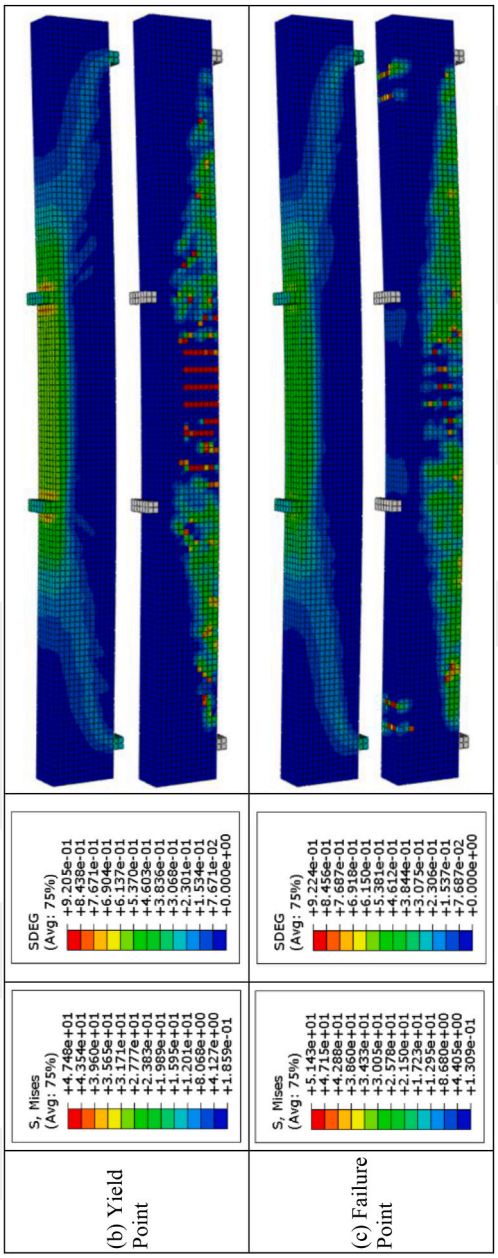

Fig. 28. Stress and SDEG graphs of the GB3F2C0 beam at yield and failure points.

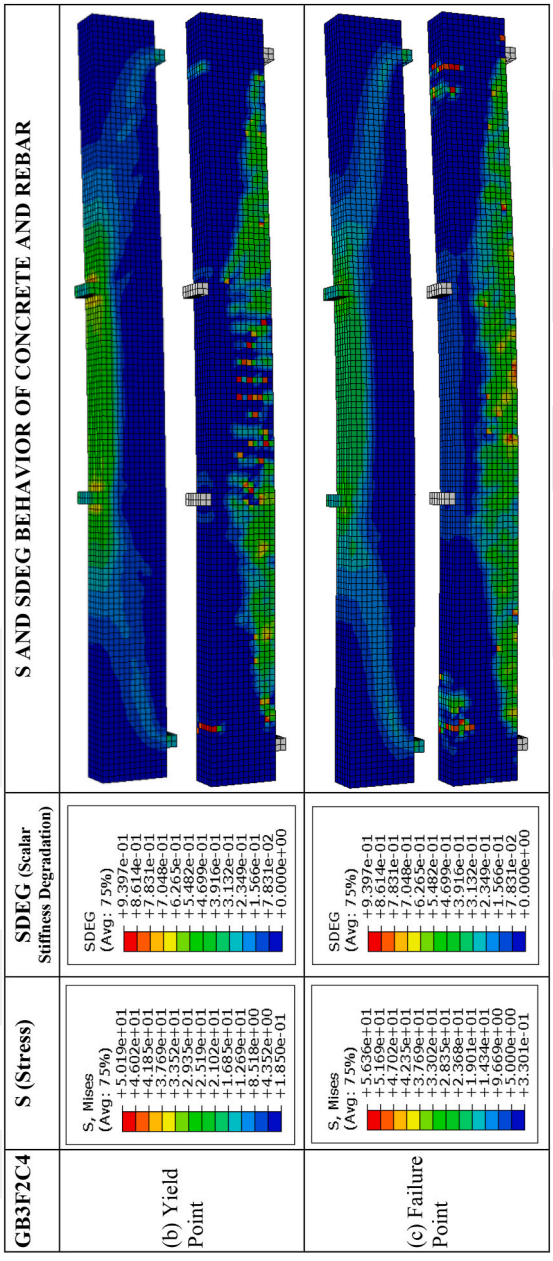

Fig. 29. Stress and SDEG graphs of the GB3F2C4 beam at yield and failure points.

Fig. 30. Stress and SDEG graphs of OPCB3 beam at yield and failure point.

reach full capacity because of the damage in the tension zone in GPC beams. For this reason, by increasing the tensile reinforcement ratio in GPC beams, the capacity of the beam compression zone can be better utilized. In addition, increasing the tensile reinforcement of GPC will provide an advantage over OPC in terms of ductility. Because GPC beams reached the ultimate state at lower deflections compared to OPC (Fig. 8). The stress values in the compression zone of the heat-cured (C4) samples after four days increased among GPC reinforced concrete beams. An increase in the SS/SH ratio also increased the stress value in the compression zone. While the stresses in the compression zone increased in all GPC beams after the yield point and reached the ultimate state, the opposite situation was observed in OPC. The damage to the compression zone of OPC was effective in the stress decrease.

In GB2-GPC beams with 3 Ø 14 tensile reinforcement, the stress values at the yield point are close to OPC beams as in GB1. However, in the ultimate state, the stress values in the average GPC beams were obtained 34 % higher than those in OPC. The stress values of the GPC beams were obtained higher in the samples that were kept for four days before thermal curing (C4) and had a SS/SH ratio of 3.5 (F2). However, GPC and OPC concrete ultimate deflections do not show any significant difference in GB2 beams. While the spread of stress towards the bottom supports is clearly seen in OPC, it is at a lower level in GPC. This situation is considered to be due to the tensile damage reaching the compression zone as a result of the lower deformation capacity of OPC concrete. As in GB1 beams, yield and ultimate damage distributions in GB2 beams tend to decrease as they are close to the bottom supports, concentrating between the two supports. However, in OPC beams, they are more homogeneously distributed throughout the entire section and, unlike GPC, in the bottom support region, including the beam section top flange. While damage occurring in the entire section does not make strengthening possible, local damage occurring in GPC seems more advantageous in terms of applying strengthening. The high deformation capacity of GPC increases energy consumption, ensures that the damage shifts to the middle region of the beam instead of the supports and makes the supports more resistant to damage. Finally, in the transition from the yield point to the ultimate state, GPC stresses increased while OPC stresses decreased as in GB1 beams.

It was determined that GPC-GB3 beams with 4 Ø 16 tension reinforcement have similar stress and damage distributions to OPC beams in both yield and ultimate states. The stresses in the beam compression zone and the distribution of these stresses towards the bottom supports overlap in all beams. In addition, when the damage distributions are investigated, it is observed that the results in the yield and ultimate states are compatible with each other. Although the stress and damage distributions are compatible with each other, the average of the GPC stress values is higher than the OPC at the time of yield and in the ultimate state, all of the GPC samples reached higher stress values compared to the OPC. As in GB1 and GB2 beams, increasing the SS/SH ratio (F2) and waiting the samples before thermal curing (C4) increased the stress values in GPC beams. The average of GPC samples showed 7.4 % higher stress behavior at the time of yielding compared to OPC and 10.4 % higher stress value at the time of failure.

Based on these results, the increase in tensile reinforcement makes the strength and behavior of GPC and OPC more similar. However, the larger stresses in GPC indicate that the stiffness reduction is slightly lower than in OPC due to the large deformation capacity. Similarly, previous studies have reported that the modulus of elasticity of GPC concrete is lower than that of OPC concrete [51–53]. Tran et al. also reported that it has the lowest cracking moment and stiffness at the post-cracking stage due to its high drying shrinkage and low modulus of elasticity, and its displacement is approximately 40 % greater than that of OPC [54]. It was concluded that the GPC tensile reinforcement ratios should be greater than those of OPC due to the lower elastic modulus of GPC and the consequently greater strain demands required to exhibit similar strength to OPC. Yost et al. [55] also reported that the deformation value in concrete at which compression failure occurs in beams with an underbalance reinforcement ratio is significantly higher than in OPC beams with similar underbalance reinforcement. In addition, according to the experimental results in the study, it was emphasized that underbalance beams exhibited equally good performance compared to OPC beams with similar concrete strength. It was reported that a similar situation was valid for crack width, flexural strength, and elastic behavior.

4. Conclusion

Numerical models were produced to be used in finite element analysis in order to make comparisons with the test data of steel reinforced GPC concrete beams produced with different activator ratios, curing techniques, and reinforcement ratios. Then, the results obtained from the FE analysis performed with the help of these models, which could not be obtained from the experimental measurements, were evaluated in terms of various design parameters, and the differences in stress and damage distributions were revealed. Thus, it is aimed to provide effective and safe data by investigating the behavioral characteristics of GPC beams in more detail through FEA without the need to test on a prototype or scale model for beam design. Additionally, it is aimed to determine the confidence percentage of the design data obtained from the FEA. In this context, the following results were reached at the end of the study.

- The closest results to the experimental data of load-displacement were obtained from beam samples with SS/SH ratio of 3.5 by the numerical models designed for GPC. The curing technique also affected the predictions of the models, especially depending on the reinforcement ratio.
- The experimental load-displacement values of the GPC beam samples were overestimated by the numerical models, indicating that the design should be on the safe side.
- GPC beams are better simulated by numerical models than OPC beams according to the load-displacement graphs.
- Although there are some differences between numerical and experimental data in moment-curvature graphs, this deviation is around 5–6%, especially in terms of yield and ultimate moment values.
- The curvature values in all samples, especially the ultimate (at failure point) curvature value, were generally estimated as underestimate by numerical models.

- It is thought that the curing method has an effect on the estimation of the moment value, and for minimum and balanced reinforced sections, C0 and for maximum reinforced sections, C4 curing technique presented closer results.
- When the numerical stress and SDEG behaviors of GPC beams were investigated, the highest value of stress was calculated from the F1C4 sample at the yield point and in the F2C4 sample at the failure point. The GPC average has similar values to OPC except for the overbalance reinforcement ratio at the yield point. All GPC samples reached a higher stress value compared to OPC at the failure point.
- The average of GPC samples showed 7.4 % higher stress behavior at the time of yielding compared to OPC and 10.4 % higher stress value at the time of failure.
- By comparing damage distributions, the stiffness reduction in OPC samples is spread homogeneously over a wider area compared to GPC, both at the yield and failure point. These damage distributions in GPC specimens, are more concentrated between local loading points. An increase in the reinforcement ratio makes this similar in terms of damage distribution.

In general, using FEA results obtained from numerical models in GPC beam design, the reinforcement ratios in the section become important. The linear stress values of GPC and OPC beams are similar, but when the non-linear plastic stage is proceeded, the maximum stress and final deformation behavior depending on the elasticity modulus of GPC are different, and accordingly, differences are observed in the stress and damage distributions in the ultimate state. These differences should be taken into account in the design, specifications, and calculations of GPC beams. Although there are similarities in terms of strength, there are some differences in behavior between GPC and OPC members. By revealing these differences through FE analysis, the specifications to be implemented for the design of GPC members can be used in applications based on faster, more reliable, and low-cost research findings.

However, there are some assumptions and limitations in both experimental setup and FEM models. The restrictions of experimental setup, laboratory condition, material and system complexity, difficulties in test procedure, and environmental factors are some limitations of experiments. On the other hand, the definition of material model and its properties, meshing, determination of boundary conditions, modelling of adhesion between the concrete and reinforcement, assumptions of analysis and design are the limitations of FE-based model analysis. In order to overcome all these difficulties, experimental validation plays an important role in FEM analysis. Mesh sensitivity analysis showed that a 25 $\times$ 25 mm mesh size provided the closest correlation with experimental results, improving the reliability of the numerical model. Thus, validated models of material and design properties help to create the assumption of boundary conditions and analysis in terms of estimation. Additionally, statistical evaluations confirmed the consistency between numerical and experimental findings, particularly in ultimate and yield load predictions. After all, geopolymer concrete beam elements can be used as an alternative structural load-bearing element to OPC beams with the optimum design and an effective reinforcement ratio. Geopolymer concrete has a higher deformation capacity compared to OPC concrete. Therefore, the use of GPC concrete can provide better performance compared to OPC. After all, geopolymer concrete beam elements can be used as an alternative structural load-bearing element to OPC beams with the optimum design and an effective reinforcement ratio. Geopolymer concrete has a higher deformation capacity compared to OPC concrete. Therefore, the use of GPC concrete can provide better performance compared to OPC.

Thanks to the microstructural properties and gel structure of GPC, better adhesion is achieved between the reinforcement and concrete, which prevents excessive stress concentrations and localizes damage. Unlike OPC, where cracks are distributed over a wider area in the form of microcracks, GPC exhibits a more localized damage pattern. This results in fewer but wider cracks, as stress is concentrated in specific regions rather than being spread homogeneously across the material. While this localized damage might suggest higher stress intensities in certain areas, it actually contributes to improved structural performance by preventing sudden and brittle failure. The gel phase in GPC absorbs energy more efficiently, leading to higher ductility and controlled crack propagation. Moreover, this behavior enhances bond strength between concrete and reinforcement, reducing early-stage crack development and delaying failure under cyclic or impact loads. The results suggest that GPC's enhanced seismic resistance and durability make it a viable alternative to OPC, especially in applications requiring high durability and energy dissipation capacity. As a result, GPC beams demonstrate better energy dissipation capacity, making them more suitable for applications requiring high durability and seismic resistance.

CRediT authorship contribution statement

Ahmet Özbayrak: Writing – review & editing, Writing – original draft, Visualization, Validation, Supervision, Resources, Project administration, Methodology, Investigation, Funding acquisition, Formal analysis, Data curation, Conceptualization. **Hurmet Kucukgoncu:** Writing – review & editing, Writing – original draft, Visualization, Validation, Supervision. **Huseyin Hilmi Aslanbay:** Writing – review & editing, Writing – original draft, Software, Resources, Methodology, Investigation. **Yuksel Gul Aslanbay:** Writing – review & editing, Writing – original draft, Visualization, Resources, Methodology, Investigation.

Declaration of competing interest

The authors declare the following financial interests/personal relationships which may be considered as potential competing interests: Ahmet reports financial support was provided by TUBITAK. If there are other authors, they declare that they have no known competing financial interests or personal relationships that could have appeared to influence the work reported in this paper.

Acknowledgments

This research was supported by TUBITAK (The Scientific and Technological Research Council of Türkiye) under grant number 121M236.

Data availability

Data will be made available on request.

References

[1] M.C. Acar, A. Şener, A. Özbayrak, A.İ. Çelik, The effect of zeolite additive on geopolymer mortars, J. Eng. Sci. Design 8 (2020) 820–832, https://doi.org/10.21923/JESD.768565.
[2] A.İ. Çelik, A. Özbayrak, A. Şener, M.C. Acar, Effect of activators in different ratios on compressive strength of geopolymer concrete, Can. J. Civ. Eng. (2022), https://doi.org/10.1139/cjce-2021-0529.
[3] F. Çeçen, A. Özbayrak, B. Aktaş, Experimental modal analysis of fly ash-based geopolymer concrete specimens via modal circles, mode indication functions, and mode shape animations, Cem. Concr. Compos. 137 (2023) 104951, https://doi.org/10.1016/J.CEMCONCOMP.2023.104951.
[4] A. Özbayrak, H. Kucukgoncu, O. Atas, H.H. Aslanbay, Y.G. Aslanbay, F. Altun, Determination of stress-strain relationship based on alkali activator ratios in geopolymer concretes and development of empirical formulations, Structures 48 (2023) 2048–2061, https://doi.org/10.1016/J.ISTRUC.2023.01.104.
[5] Y.G. Aslanbay, H.H. Aslanbay, A. Özbayrak, H. Kucukgoncu, O. Atas, Comprehensive analysis of experimental and numerical results of bond strength and mechanical properties of fly ash based GPC and OPC concrete, Constr. Build. Mater. 416 (2024), https://doi.org/10.1016/j.conbuildmat.2024.135175.
[6] A. Özbayrak, H. Kucukgoncu, H.H. Aslanbay, Y.G. Aslanbay, O. Atas, Comprehensive experimental analysis of the effects of elevated temperatures in geopolymer concretes with variable alkali activator ratios, J. Build. Eng. 68 (2023), https://doi.org/10.1016/J.JOBE.2023.106108.
[7] S. Venkatachalam, K. Vishnuvardhan, G.D. Amarapathi, S.R. Mahesh, M. Deepasri, Experimental and finite element modelling of reinforced geopolymer concrete beam, in: Mater Today Proc, 2020, pp. 6500–6506, https://doi.org/10.1016/j.matpr.2020.11.449.
[8] B. Abdelwahed, Nonlinear numerical simulation for reinforced concrete elements with explicit time integration procedure, Case Stud. Constr. Mater. 12 (2020) e00344, https://doi.org/10.1016/J.CSCM.2020.E00344.
[9] F. Korkut, M. Karalar, Investigational and numerical examination on bending response of reinforced rubberized concrete beams including plastic waste, Materials 16 (2023) 5538, https://doi.org/10.3390/MA16165538, 16 (2023) 5538.
[10] M. Abubakar, Numerical investigation of reinforced concrete beam contain-ing iron ore tailings as partial replacement of sand, Ethiop.Int. J. Eng. Technol. 1 (2023) 66–77, https://doi.org/10.59122/144cfc18.
[11] A. Hassan, M. Arif, M. Shariq, T. Alomayri, Experimental test and finite element modelling prediction on geopolymer concrete beams subject to flexural loading, Innovative Infrastruct. Solut. 7 (2022) 1–18, https://doi.org/10.1007/S41062-021-00615-9/FIGURES/25.
[12] A. Tambusay, B. Suryanto, K. Chong, P. Suprobo, Nonlinear analysis of reinforced geopolymer concrete beams, Civil Eng. Dimension 24 (2022) 1–10, https://doi.org/10.9744/ced.24.1.1-10.
[13] M.W. Aziz, P. Suprobo, Y. Tajunnisa, Numerical analysis study of the effect geopolymer concrete compressive strength on ductility of reinforced concrete beams, J. Civ. Eng. 37 (2022) 33, https://doi.org/10.12962/j20861206.v37i1.12193.
[14] N.O. Nofal, H.H. Ahmed, G.A. Hamdy, A.S. Shanour, S.G. Saad, Flexural behavior of steel and FRP-reinforced geopolymer concrete beams : numerical modeling and analytical study, Eng. Res.J. (2023) 38–47.
[15] J. Liu, F. Yan, Experimental investigation and numerical simulation of the flexural behavior of reinforced concrete beams strengthened by geopolymer-bonded CFRP, Multidiscip. Model. Mater. Struct. 18 (n.d.) 401–429. https://doi.org/10.1108/MMMS-04-2022-0049.
[16] A. İhsan Çelik, A. Özbayrak, A. Şener, M.C. Acar, Numerical analysis of flexural and shear behaviors of geopolymer concrete beams Journal of Sustainable Construction Materials and Technologies, J Sustain Const Mater Technol 7 (2022) 70–80, https://doi.org/10.47481/jscmt.1116561.
[17] M.S. Darmawan, Y. Tajunnisa, P. Suprobo, W. Sutrisno, M.W. Aziz, Comparative study of flexural performance of geopolymer and portland cement concrete beam using finite element analysis, Geomat. J 23 (2022) 1–9, https://doi.org/10.21660/2022.95.j2340.
[18] Y.N. Wibowo, B. Piscesa, Y. Tajunnisa, Numerical investigation of geopolymer reinforced concrete beams under flexural loading using 3DNLFEA, J. Civ. Eng. 37 (2022) 27, https://doi.org/10.12962/j20861206.v37i1.12095.
[19] N.A.M. Mortar, M.M. Al Bakri Abdullah, K. Hussin, R.A. Razak, S. Hamat, A.H. Hilmi, N.N. Shahedan, L.Y. Li, I.H.A. Aziz, Finite element analysis on structural behaviour of geopolymer reinforced concrete beam using johnson-cook damage in ABAQUS, Arch. Metall. Mater. 67 (2022) 1349–1354, https://doi.org/10.24425/amm.2022.141061.
[20] A.G. Alex, T. Gebrehiwet Tewele, Z. Kemal, R.B. Subramanian, Flexural behavior of low calcium fly ash based geopolymer reinforced concrete beam, Int J Concr Struct Mater 16 (2022), https://doi.org/10.1186/s40069-022-00531-x.
[21] H. Kucukgoncu, A. Özbayrak, Microstructural analysis of low-calcium fly ash-based geopolymer concrete with different ratios of activator and binder under high temperatures, Arabian J. Sci. Eng. (2024) 1–27, https://doi.org/10.1007/S13369-024-09266-1/FIGURES/1.
[22] ASTM C311, Standard Test Methods for Sampling and Testing Fly Ash or Natural Pozzolans for Use, 2003. West Conshohocken, Pennsylvania, USA.
[23] ACI318-14, 318-14, Building Code Requirements for Structural Concrete and Commentary, 2014, https://doi.org/10.14359/51688187. Farmington Hills, MI 48331, U.S.A.
[24] A. Sathonsaowaphak, P. Chindaprasirt, K. Pimraksa, Workability and strength of lignite bottom ash geopolymer mortar, J. Hazard Mater. 168 (2009) 44–50, https://doi.org/10.1016/j.jhazmat.2009.01.120.
[25] J.C. Swanepoel, C.A. Strydom, Utilisation of fly ash in a geopolymeric material, Appl. Geochem. 17 (2002) 1143–1148, https://doi.org/10.1016/S0883-2927(02)00005-7.
[26] U. Rattanasak, P. Chindaprasirt, Influence of NaOH solution on the synthesis of fly ash geopolymer, Miner. Eng. 22 (2009) 1073–1078, https://doi.org/10.1016/j.mineng.2009.03.022.
[27] Y.X. Ma, O. Zhao, K.H. Tan, Experimental and numerical studies of concrete-encased concrete-filled steel tube stub columns under uniaxial and biaxial eccentric compression, Eng. Struct. 232 (2021) 111796, https://doi.org/10.1016/J.ENGSTRUCT.2020.111796.
[28] TS-500, Requirements for Design and Construction of Reinforced Concrete Structures, Türkiye, Ankara, 2000.
[29] ABAQUS v6.12, User's Manual, Dassault Systemes Simulia Corperation, 2018.
[30] A. Khennane, Introduction to finite element analysis using MATLAB® and abaqus. https://doi.org/10.1201/b15042, 2013.
[31] A. Demir, N. Caglar, H. Ozturk, Y. Sumer, Nonlinear finite element study on the improvement of shear capacity in reinforced concrete T-Section beams by an alternative diagonal shear reinforcement, Eng. Struct. 120 (2016) 158–165, https://doi.org/10.1016/J.ENGSTRUCT.2016.04.029.
[32] K. Cichocki, J. Domski, J. Katzer, M. Ruchwa, Mechanical properties and numerical approach to fibre reinforced wca concrete slabs, in: Brittle Matrix Composites 11 - Proceedings of the 11th International Symposium on Brittle Matrix Composites BMC 2015, 2015, pp. 309–318.
[33] O. Martin, Comparison of different constitutive models for concrete in ABAQUS/explicit for missile impact analyses. https://doi.org/10.2790/19763, 2010.
[34] J. Lubliner, J. Üliver, S. Üller, E. Üñate, Plastic-damage model for concrete, Int. J. Rock Mech. Min. Sci. Geomech. Abstracts 26 (1989) 252, https://doi.org/10.1016/0148-9062(89)91126-1.

[35] J. Lee, G.L. Fenves, Plastic-damage model for cyclic loading of concrete structures, J. Eng. Mech. 124 (1998) 892–900, https://doi.org/10.1061/(asce)0733-9399(1998)124:8(892).
[36] H. Ma, H. Wang, Z. Li, X. Sun, X. Zhang, The finite element analysis of RC energy absorption columns based on ABAQUS software, in: Applied Mechanics and Materials, Trans Tech Publications Ltd, 2012, pp. 2122–2125, https://doi.org/10.4028/www.scientific.net/AMM.174-177.2122.
[37] W. Ren, L.H. Sneed, Y. Yang, R. He, Numerical simulation of prestressed precast concrete bridge deck panels using damage plasticity model, Int J Concr Struct Mater 9 (2015) 45–54, https://doi.org/10.1007/s40069-014-0091-2.
[38] B. Mercan, A.E. Schultz, H.K. Stolarski, Finite element modeling of prestressed concrete spandrel beams, Eng. Struct. 32 (2010) 2804–2813, https://doi.org/10.1016/j.engstruct.2010.04.049.
[39] P. Grassl, Modelling of dilation of concrete and its effect in triaxial compression, Finite Elem. Anal. Des. 40 (2004) 1021–1033, https://doi.org/10.1016/j.finel.2003.04.002.
[40] O.H. Zinkaah, Z. Alridha, M. Alhawat, Numerical and theoretical analysis of FRP reinforced geopolymer concrete beams, Case Stud. Constr. Mater. 16 (2022) e01052, https://doi.org/10.1016/J.CSCM.2022.E01052.
[41] A. Fuzail Hashmi, M. Shariq, A. Baqi, Flexural performance of high volume fly ash reinforced concrete beams and slabs, Structures 25 (2020) 868–880, https://doi.org/10.1016/J.ISTRUC.2020.03.071.
[42] G. George, P.K. Shreeram, A.S. Minalan, K. Lokesh, M. Mano, A. Prince, Numerical investigation on the flexural behavior of geopolymer concrete beam reinforced with different types of fiber-reinforced polymer bars, Mater. Today Proc. (2023), https://doi.org/10.1016/J.MATPR.2023.04.049.
[43] K.B. S.E. Hibbitt H. D.I., ABAQUS User's Manual. Providence (RI), Dassault Systemes Simulia Corp, 2013.
[44] A.Z. Kamali, Shear Strength of Reinforced Concrete Beams Subjected to Blast Loading, 2012.
[45] V. Birtel, P. Mark, Parameterised finite element modelling of RC beam shear failure, Ababqus User's Conference (2006) 95–108.
[46] W.B. Krätzig, R. Pölling, An elasto-plastic damage model for reinforced concrete with minimum number of material parameters, Comput. Struct. 82 (2004) 1201–1215, https://doi.org/10.1016/j.compstruc.2004.03.002.
[47] A. Earij, G. Alfano, K. Cashell, X. Zhou, Nonlinear three–dimensional finite–element modelling of reinforced–concrete beams: computational challenges and experimental validation, Eng. Fail. Anal. 82 (2017) 92–115, https://doi.org/10.1016/j.engfailanal.2017.08.025.
[48] F. Lopez-Almansa, B. Alfarah, S. Oller, Numerical simulation of RC frame testing with damaged plasticity model comparison with simplified models. 2nd European Conference on Earthquake Engineering and Seismology, 2014, pp. 1–12.
[49] J.B. Mander, M.J.N. Priestley, R. Park, Theoretical stress-strain model of confined concrete, J. Struct. Eng. 114 (1988) 1804–1826.
[50] J.A.L. Pipa, Elements Subjected to Cyclical Actions, Influence of the Mechanical Characteristics of the Rebar, Universidade Técnica de Lisboa, Instituto Superior Técnico, 1993. PhD Thesis.
[51] A. Noushini, F. Aslani, A. Castel, R.I. Gilbert, B. Uy, S. Foster, Compressive stress-strain model for low-calcium fly ash-based geopolymer and heat-cured Portland cement concrete, Cem. Concr. Compos. 73 (2016) 136–146, https://doi.org/10.1016/J.CEMCONCOMP.2016.07.004.
[52] Z. Pan, J.G. Sanjayan, B.V. Rangan, Fracture properties of geopolymer paste and concrete, Mag. Concr. Res. 63 (2011) 763–771, https://doi.org/10.1680/MACR.2011.63.10.763.
[53] A.M. Fernández-Jiménez, A. Palomo, C. López-Hombrados, Engineering properties of alkali-activated fly ash concrete, ACI Mater. J. 103 (2006) 106–112, https://doi.org/10.14359/15261.
[54] T.T. Tran, T.M. Pham, H. Hao, Experimental and analytical investigation on flexural behaviour of ambient cured geopolymer concrete beams reinforced with steel fibers, Eng. Struct. 200 (2019) 109707, https://doi.org/10.1016/j.engstruct.2019.109707.
[55] J.R. Yost, A. Radlińska, S. Ernst, M. Salera, N.J. Martignetti, Structural behavior of alkali activated fly ash concrete. Part .Structural testing and experimental findings, Mater. Struct. Mater. et Construct. 46 (2013) 449–462, https://doi.org/10.1617/s11527-012-9985-0.